© Pol J Radiol 2022; 87: e141-e162
DOI: https://doi.org/10.5114/pjr.2022.113825

Received: 30.09.2021
Accepted: 27.10.2021
Published: 05.03.2022

Polish Journal of Radiology

http://www.polradiol.com

Review paper

Magnetic resonance imaging of musculoskeletal infections

Jennifer S. Weaver[1,A,B,C,D,E,F], Imran M. Omar[2,E], Winnie A. Mar[3,E], Andrea S. Klauser[4,E], Blair A. Winegar[5,E], Gary W. Mlady[1,E], Wendy E. McCurdy[6,E], Mihra S. Taljanovic[1,7,A,B,C,D,E,F]

[1]Department of Radiology, University of New Mexico School of Medicine, Albuquerque, New Mexico, USA
[2]Department of Radiology, Northwestern University Feinberg School of Medicine, Chicago, Illinois, USA
[3]Department of Radiology, University of Illinois at Chicago, Chicago, Illinois, USA
[4]Department of Radiology, Medical University of Innsbruck, Innsbruck, Austria
[5]Department of Radiology, University of Utah School of Medicine, Salt Lake City, Utah, USA
[6]Department of Medical Imaging, University of Arizona, Tuscon, Arizona, USA
[7]Departments of Medical Imaging and Orthopaedic Surgery, University of Arizona, Tucson, Arizona, USA

Abstract

Magnetic resonance imaging (MRI) is a powerful imaging modality in the evaluation of musculoskeletal (MSK) soft tissue, joint, and bone infections. It allows prompt diagnosis and assessment of the extent of disease, which permits timely treatment to optimize long-term clinical outcomes. MRI is highly sensitive and specific in detecting the common findings of MSK infections, such as superficial and deep soft tissue oedema, joint, bursal and tendon sheath effusions, lymphadenopathy, bone marrow oedema, erosive bone changes and periostitis, and bone and cartilage destruction and sequestration. Contrast-enhanced MRI allows detection of non-enhancing fluid collections and necrotic tissues, rim-enhancing abscesses, heterogeneously or diffusely enhancing phlegmons, and enhancing active synovitis. Diffusion-weighted imaging (DWI) is useful in detecting soft-tissue abscesses, particularly in patients who cannot receive gadolinium-based intravenous contrast. MRI is less sensitive than computed tomography (CT) in detecting soft-tissue gas. This article describes the pathophysiology of pyogenic MSK infections, including the route of contamination and common causative organisms, typical MR imaging findings of various soft tissue infections including cellulitis, superficial and deep fasciitis and necrotizing fasciitis, pyomyositis, infectious bursitis, infectious tenosynovitis, and infectious lymphadenitis, and of joint and bone infections including septic arthritis and osteomyelitis (acute, subacute, and chronic). The authors also discuss MRI findings and pitfalls related to infected hardware and diabetic foot infections, and briefly review standards of treatment of various pyogenic MSK infections.

Key words: MRI, osteomyelitis, septic arthritis, cellulitis, pyomyositis, fasciitis.

Introduction

Magnetic resonance imaging (MRI) is frequently used to diagnose soft tissue and bone infections, to determine the extent of disease, and to exclude mimickers of infection (Figures 1-18). Signs, symptoms, and clinical examination findings of bone and soft tissue infections can be nonspecific, and laboratory values can be inconclusive, making it clinically difficult to confirm the presence and extent of disease [1]. Early diagnosis and prompt initiation of treatment can optimize long-term clinical outcomes in patients with musculoskeletal (MSK) infections. Delays in diagnosis and treatment can lead to structural damage as well as disease spread to other organ systems, increasing morbidity and mortality.

Soft tissue and bone infections most commonly occur secondarily to broken skin from trauma, surgery, or diabetic ulcers; infections can also occur from haematogenous

Correspondence address:
Dr. Jennifer S. Weaver, Department of Radiology, University of New Mexico, MSC 10 5530, Albuquerque, NM, 87131, USA, e-mail: jsweaver@salud.unm.edu

Authors' contribution:
A Study design · **B** Data collection · **C** Statistical analysis · **D** Data interpretation · **E** Manuscript preparation · **F** Literature search · **G** Funds collection

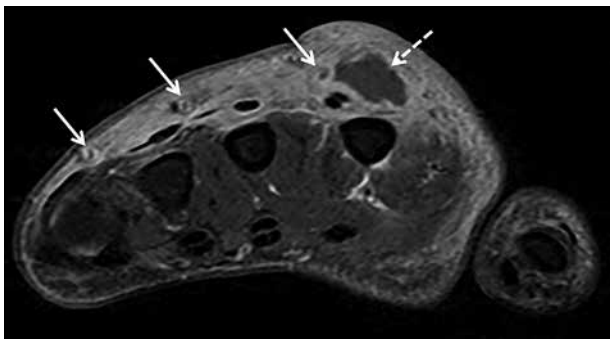

Figure 1. A 46-year-old female intravenous drug user with right hand cellulitis, subcutaneous abscess, and septic superficial thrombophlebitis. Axial T1-weighted magnetic resonance image with fat saturation post intravenous gadolinium-based contrast shows heterogeneous enhancement of the right hand dorsal subcutaneous tissues related to cellulitis with a rim-enhancing abscess (dashed arrow) and multiple small rim-enhancing superficial veins with central non-enhancement consistent with septic thrombophlebitis (solid arrows)

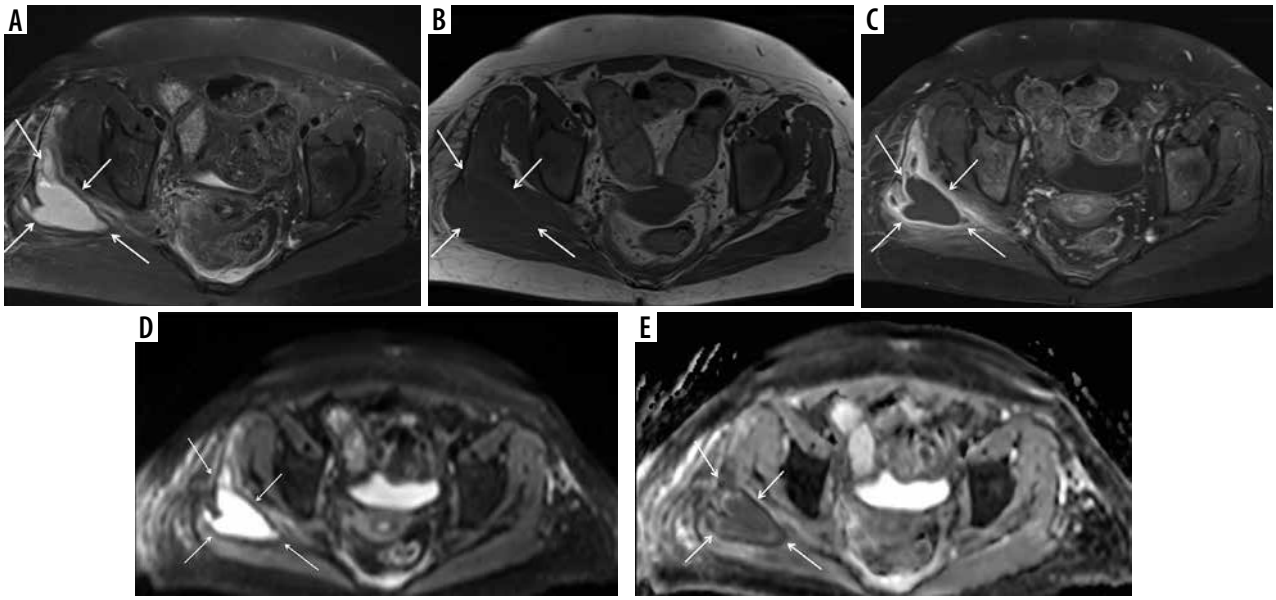

Figure 2. A 50-year-old female with myeloid leukaemia on chemotherapy, with neutropaenia and right gluteal infection with soft-tissue abscess. **A)** Axial T2-weighted magnetic resonance image with fat saturation shows high signal intensity lobulated intramuscular right gluteal fluid collection (arrows) with surrounding patchy high-signal muscular oedema and overlying subcutaneous oedema. **B)** The fluid collection shows intermediate signal intensity on the axial T1-weighted MR image without fat saturation (arrows) with higher signal intensity rim consistent with penumbra sign. Note diffuse decreased bone marrow signal intensity in keeping with myeloid leukaemia. **C)** On the axial T1-weighted MR image with fat saturation post intravenous gadolinium-based contrast administration the lesion shows rim enhancement and no internal enhancement consistent with an abscess. Note heterogeneously enhancing surrounding muscular oedema consistent with myositis/phlegmon. DWI MRI shows high signal intensity within the intramuscular abscess in (**D**) axial fractional anisotropy/trace image and restricted diffusion with low signal intensity in (**E**) ADC map image. Surrounding myositis and overlying cellulitis show heterogeneous high signal intensity in both **(D)** and **(E)** consistent with T2 shine-through effect. In (**A**), (**D**), and (**E**) note a small amount of high signal intensity pre-sacral oedema

spread [1-3]. Risk factors for soft tissue and bone infections include immunosuppression, extremes of age, substance abuse, systemic illnesses, malnutrition, obesity, trauma, surgery, and burns [1].

Clinically, patients with MSK infections often present with pain, erythema, oedema, fever, and occasionally sepsis [1, 3]. Crepitus may occur if soft tissue gas is present [1, 3]. Laboratory analysis includes markers for infection: elevated white blood cells, C-reactive protein, and erythrocyte sedimentation levels [1]. Blood cultures and cultures of infected tissue allow for diagnosis of specific organisms.

The American College of Radiology (ACR) appropriateness criteria lists MRI as "usually appropriate" following radiographs for the evaluation of MSK infections, including suspected osteomyelitis, septic arthritis, and soft tissue infections, as well as suspected osteomyelitis of the foot in patients with diabetes mellitus [4, 5].

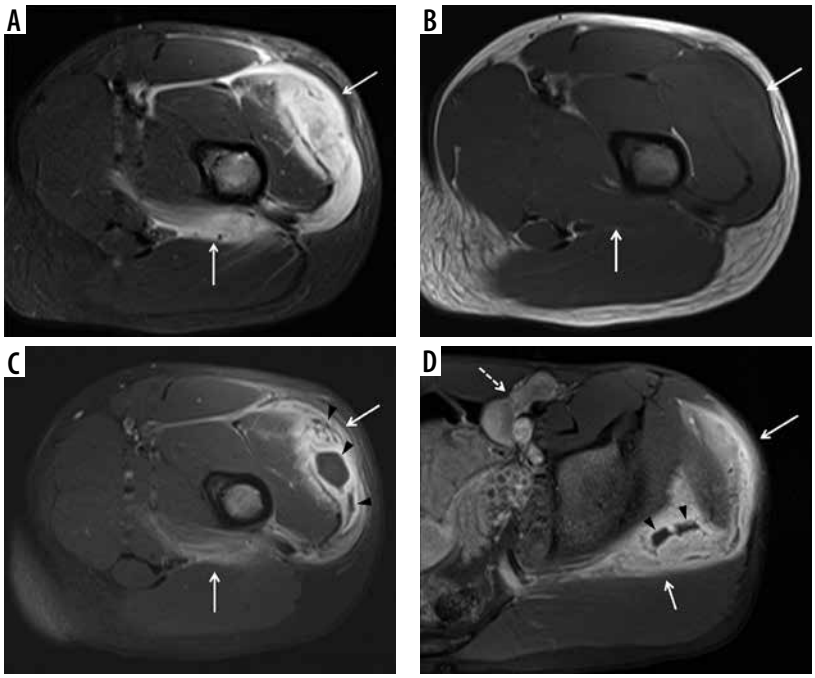

Figure 3. A 13-year-old male with sensory neuropathy and left thigh pyomyositis, fasciitis, and lymphadenitis. **A)** Axial STIR magnetic resonance (MR) image shows heterogeneous high signal intensity of the vastus lateralis and quadratus femoris musculature (arrows) with oedema in the adjacent deep fascial planes, which show intermediate signal in **(B)**. Axial T1-weighted MR image (arrows). **C)** Axial T1-weighted MR image with fat saturation post intravenous gadolinium-based contrast shows avid heterogeneous enhancement of the affected musculature and deep fascial planes consistent with pyomyositis (arrows) and deep fasciitis with several non-enhancing intramuscular abscesses in the vastus lateralis muscle (arrowheads). **D)** Axial T1-weighted magnetic resonance MR image with fat saturation post intravenous gadolinium-based contrast shows avid heterogeneous enhancement of the gluteus medius muscle consistent with pyomyositis (solid arrows) with 2 small non-enhancing intramuscular abscesses (arrowheads). Note heterogeneously enhancing moderate inguinal lymphadenopathy (dashed arrow)

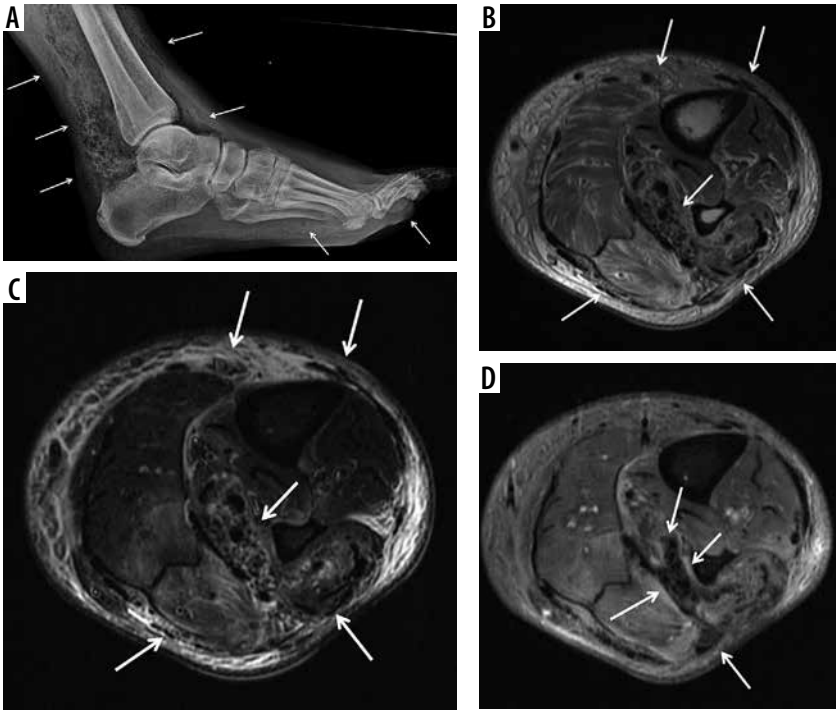

Figure 4. Necrotizing fasciitis in a 63-year-old male with poorly controlled diabetes mellitus type II, recurrent pedal soft tissue infections and osteomyelitis, and peripheral neuropathy. The patient was admitted to the ICU with fevers and worsening left lower extremity pain and swelling for 2 days, and had a nonhealing ulcer along the plantar surface of the foot. **A)** Lateral foot radiograph shows extensive soft tissue gas in the distal lower leg and plantar forefoot (arrows). There is plantar cutaneous ulceration over the metatarsophalangeal joints. **B)** Axial proton density-weighted without fat saturation and **(C)** axial T2-weighted with fat suppression magnetic resonance images of the mid lower leg show extensive areas of superficial and intermuscular fascial low signal intensity foci, consistent with soft tissue gas (arrows). This is associated with areas of patchy muscle oedema consistent with myositis, and circumferential subcutaneous oedema in keeping with cellulitis. **D)** Axial T1-weighted MR image with fat saturation post intravenous gadolinium-based contrast of the same region shows a non-enhancing area along the intermuscular facia of the posterior compartment associated with foci of gas consistent with necrosis (arrows). Mild peripheral enhancement is present, consistent with fasciitis. Note, heterogeneous muscular and subcutaneous soft tissue enhancement consistent with myositis and cellulitis. Together, these findings are highly concerning for soft-tissue infection with a gas-forming organism. Cultures from a subsequent emergent surgical debridement yielded polymicrobial infection, including *Pseudomonas aeruginosa*

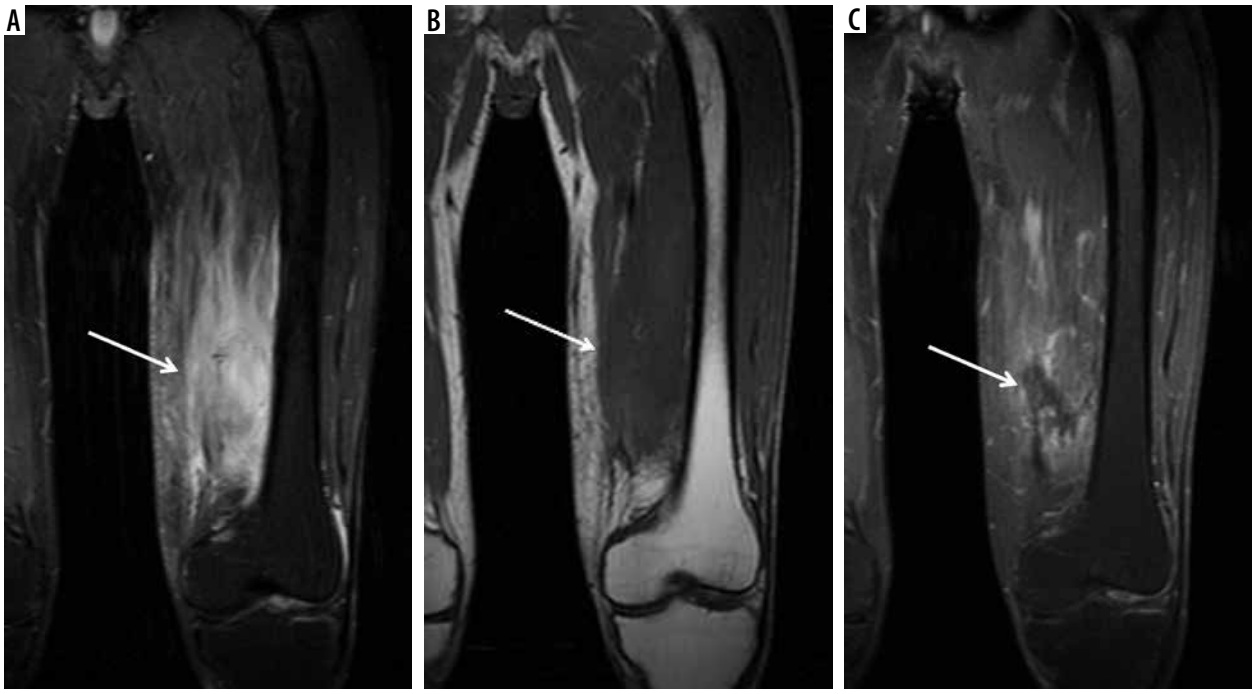

Figure 5. A 44-year-old male with left thigh pain related to diabetic myonecrosis. **A)** Coronal STIR magnetic resonance (MR) image shows markedly increased signal intensity involving the mildly enlarged anteromedial left thigh musculature (arrow) with overlying mild subcutaneous oedema, which demonstrates intermediate signal intensity isointense to skeletal muscle in **(B)** coronal T1-weighted MR image. **C)** Coronal T1-weighted MR image with fat saturation post intravenous administration of gadolinium-based contrast shows an irregular non-enhancing area of myonecrosis with mildly enhancing affected surrounding anteromedial left thigh musculature related to granulation tissue and myositis

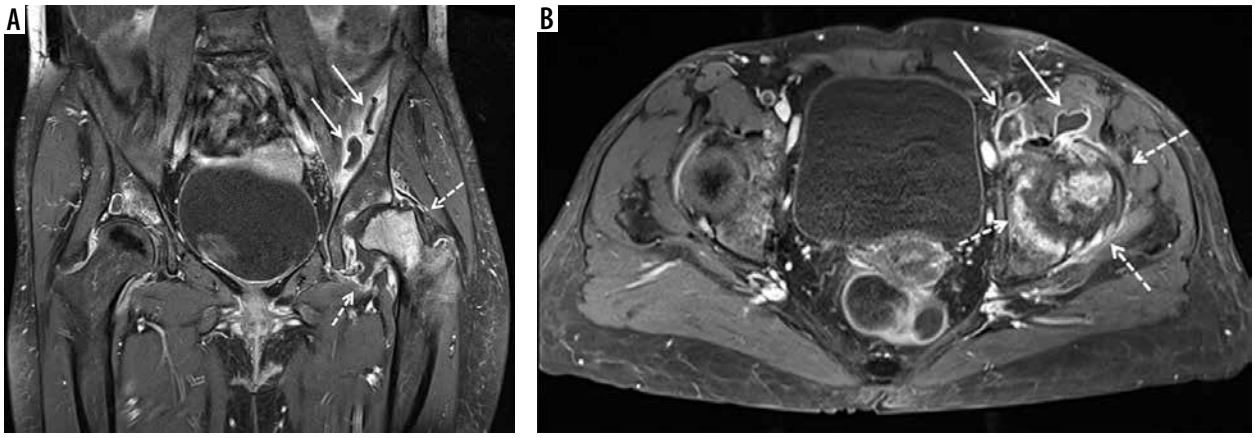

Figure 6. A 55-year-old female with septic arthritis and osteomyelitis of the left hip with associated septic iliopsoas bursitis. **A)** Coronal and **(B)** axial T1-weighted magnetic resonance image with fat saturation post intravenous gadolinium-based contrast shows left hip joint space narrowing, cortical erosions, and mild lateral subluxation of the femoral head with avid bone marrow enhancement of the femoral head and neck, and to a lesser extent of the acetabulum, and moderate distension of the joint capsule with irregular thick synovial enhancement and non-enhancing fluid consistent with septic arthritis and osteomyelitis (dashed arrows). Note moderate distension of the communicating left iliopsoas bursa with thick enhancing synovitis and non-enhancing fluid consistent with septic bursitis (solid arrows)

The high contrast and spatial resolution of MRI allows detailed evaluation of all MSK tissues. MRI is highly sensitive and specific in detecting the common findings of MSK infections, such as superficial and deep soft tissue oedema, joint, bursal and tendon sheath effusions, lymphadenopathy, bone marrow oedema, erosive bone changes and periostitis, and bone and cartilage destruction and sequestration. MRI has higher sensitivities than specificities in the evaluation of MSK infections, because several inflammatory conditions and neoplasms may have a similar MRI appearance. MRI has a 100% negative predictive value in excluding an MSK infection. Intravenously administered gadolinium-based contrast agents help to distinguish enhancing active synovitis from non-enhancing inactive synovial proliferation and joint effusions. Whole-body MRI is useful for evaluating multifocal MSK infections. Organized soft tissue, and intraosseous and subperiosteal abscesses show rim enhancement, while actively inflamed bone marrow, periostitis, and various superficial and deep soft tissues show diffuse or heteroge-

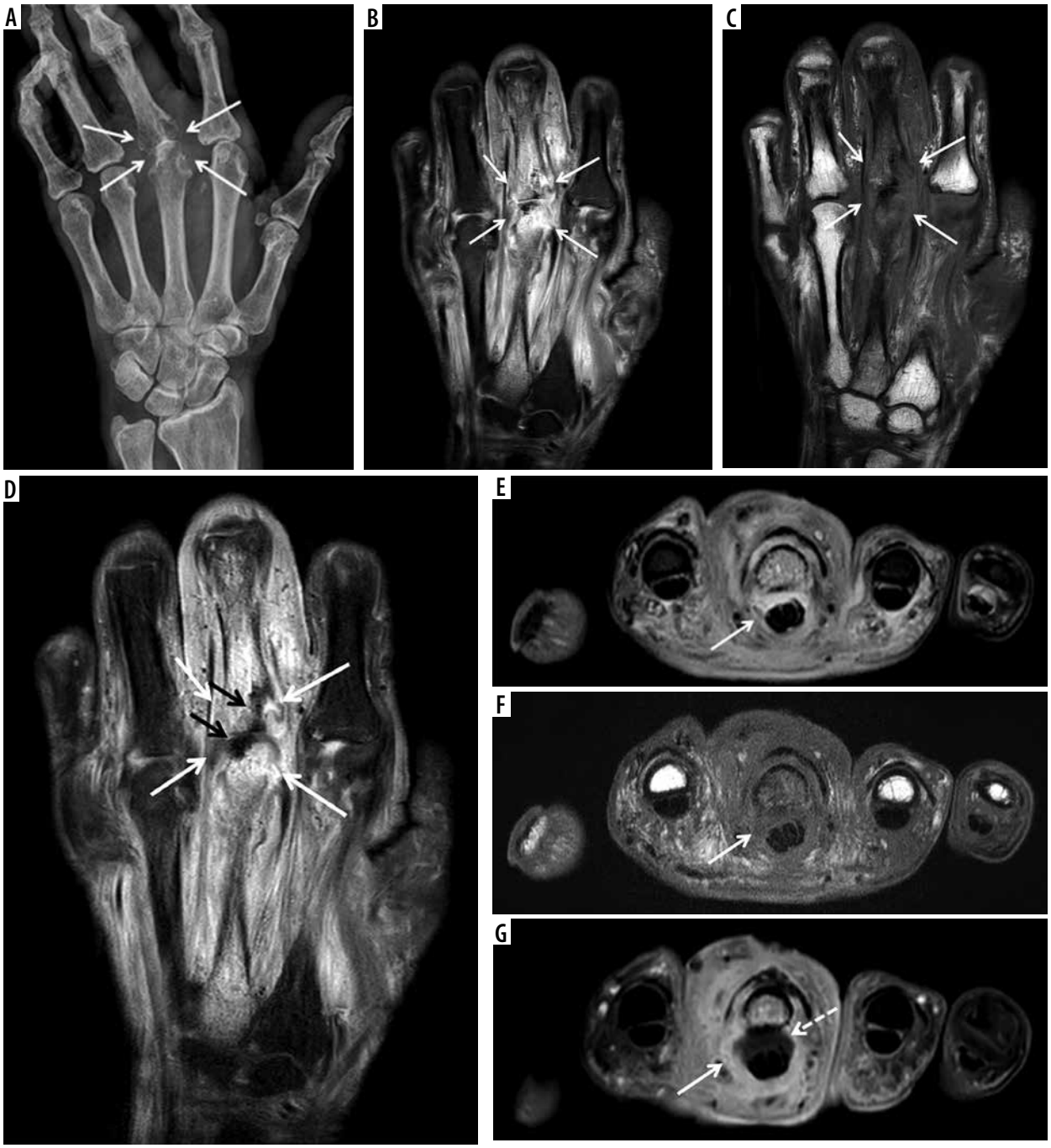

Figure 7. A 59-year-old male with uncontrolled diabetes mellitus, methicillin-susceptible *Staphylococcus aureus* and Group A streptococcal septic arthritis and osteomyelitis of the left middle finger metacarpophalangeal (MCP) joint, cellulitis, and septic tenosynovitis. **A)** Posteroanterior radiograph shows marked narrowing of the 3rd MCP joint with erosive bone changes along the metacarpal head and proximal phalangeal base consistent with septic joint and osteomyelitis. **B)** Coronal proton density-weighted magnetic resonance (MR) image with fat saturation shows narrowing of the 3rd MCP joint with erosive bone changes along the articular surfaces and marked high signal intensity bone marrow oedema involving the near entire 3rd metacarpal and proximal phalanx with associated periarticular periosteal thickening (arrows). Note associated extensive high signal intensity soft tissue oedema. The affected bone structures show low signal intensity with bone marrow effacement in **(C)** coronal T1-weighted MR image (arrows). **D)** Coronal T1-weighted MR image with fat saturation post intravenous gadolinium-based contrast shows marked enhancement of the affected bones with erosive bone changes about the 3rd MCP joint (white arrows), consistent with septic joint and osteomyelitis. Note serpiginous area of non-enhancement extending over the joint space consistent with necrotic bone (black arrows). There is additional extensive enhancement of the affected infected soft tissues. **E)** Axial proton density-weighted MR image with fat saturation shows high signal bone marrow oedema in the third proximal phalanx, high signal overlying soft tissue oedema, and a mildly distended middle finger flexor tenon sheath with heterogeneous increased signal intensity synovial-fluid complex (arrow). **F)** Axial T1-weighted MR image shows bone marrow effacement of the 3rd proximal phalanx with decreased intermediate signal in the overlying soft tissues including the flexor tendon sheath (arrow). **G)** Axial T1-weighted MR image with fat saturation post intravenous gadolinium-based contrast shows enhancement of the affected bony and soft tissue structures with thick synovial enhancement of the middle finger flexor tendon sheath (solid arrow) and a small amount of non-enhancing peritendinous fluid (dashed arrow) consistent with septic tenosynovitis

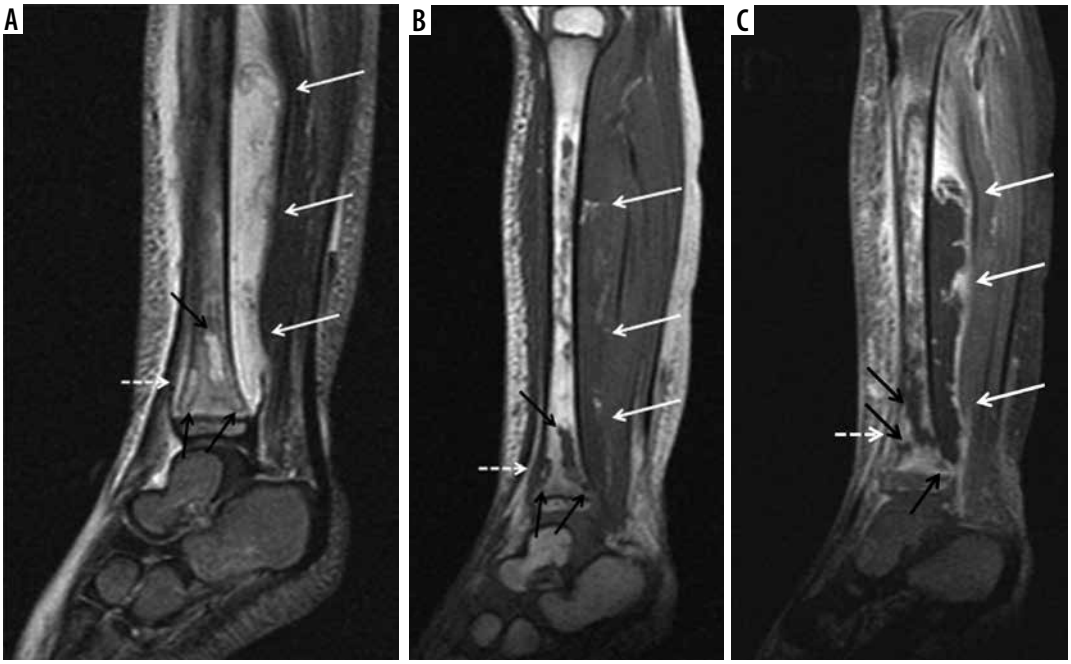

Figure 8. A 3-year-old male with *Staphylococcus aureus* acute osteomyelitis and subperiosteal abscess of the left tibia. **A)** Sagittal STIR magnetic resonance (MR) image shows heterogeneous increased signal intensity involving the left tibia throughout the bone marrow with several higher signal intensity intraosseous abscesses (black arrows), large heterogeneous high signal intensity posterior subperiosteal collection/abscess (solid white arrows), and high signal intensity periostitis along the distal tibial diametaphysis (dashed white arrow). Note high signal intensity in the overlying soft tissues related to cellulitis. **B)** On the sagittal T1-weighted MR image the intraosseous (black arrows) and subperiosteal (solid white arrows) abscesses and the anterior distal tibial periosteal thickening (dashed white arrow) show heterogeneous decreased signal intensity. Note serpiginous proximal extension of decreased signal intensity throughout the tibial diaphysis with interspersed preserved bone marrow fat of high signal intensity, which is frequently seen in acute osteomyelitis. **C)** Sagittal T1-weighted MR image with fat saturation post intravenous gadolinium-based contrast shows heterogeneous bone marrow enhancement throughout the majority of the tibia with non-enhancing intraosseous abscesses, rim enhancing large posterior subperiosteal abscess with central non-enhancement (solid white arrows), and enhancing distal diametaphyseal periostitis (dashed white arrow). Note heterogeneously enhancing overlying cellulitis

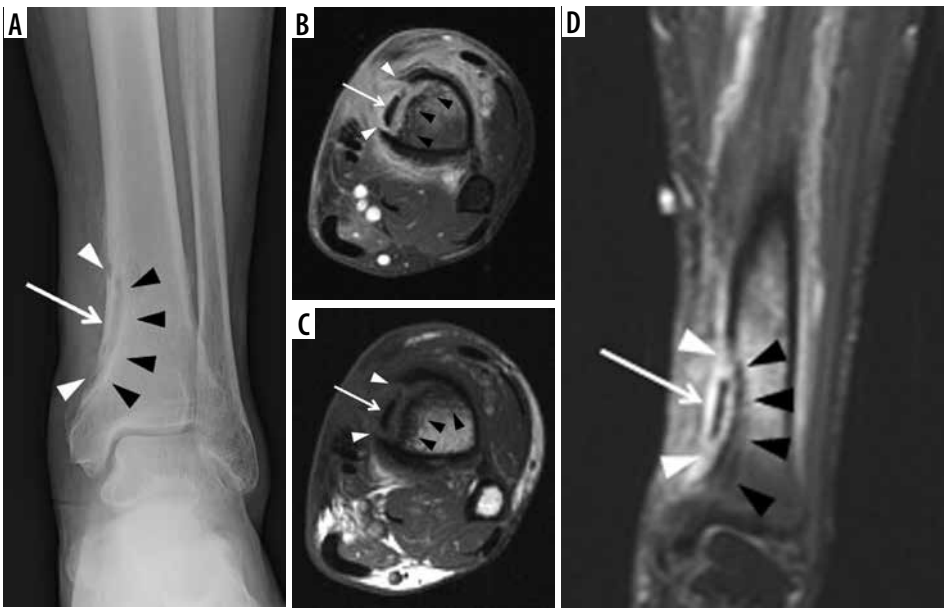

Figure 9. A 54-year-old male with chronic active polymicrobial including methicillin-resistant *Staphylococcus aureus* osteomyelitis at the medial aspect of the left distal tibia with overlying cellulitis after a burn 1 year ago. **A)** Anteroposterior radiograph shows a linear area of sclerosis at the periphery of the distal medial tibial metaphysis consistent with a sequestrum (arrow) with associated cortical defect/cloaca (between white arrowheads) and curvilinear lucency along the lateral aspect related to infection cavity with overlying reactive sclerosis/new bone formation related to involucrum (black arrowheads). **B)** Axial STIR magnetic resonance (MR) image shows low signal intensity sequestrum (arrow) with surrounding high signal intensity infection cavity, cortical defect/cloaca (between the white arrowheads), overlying central ill-defined low signal/involucrum (black arrowheads), adjacent high signal bone marrow oedema, and overlying high signal soft tissue oedema. **C)** On the axial T1-weighted MR image, note low signal intensity sequestrum (arrow) surrounded by intermediate signal infection cavity with medial cortical defect/cloaca and inner area of ill-defined low signal intensity involucrum (black arrowheads). **D)** Coronal T1-weighted MR image with fat saturation post intravenous gadolinium-based contrast shows non-enhancing low signal intensity sequestrum surrounded by avidly enhancing phlegmon with medial cortical defect/cloaca (between white arrowheads) and mildly heterogeneously enhancing involucrum at the lateral aspect (black arrowheads) with adjacent enhancing bone marrow oedema. Note heterogeneously enhancing overlying soft tissue oedema consistent with cellulitis

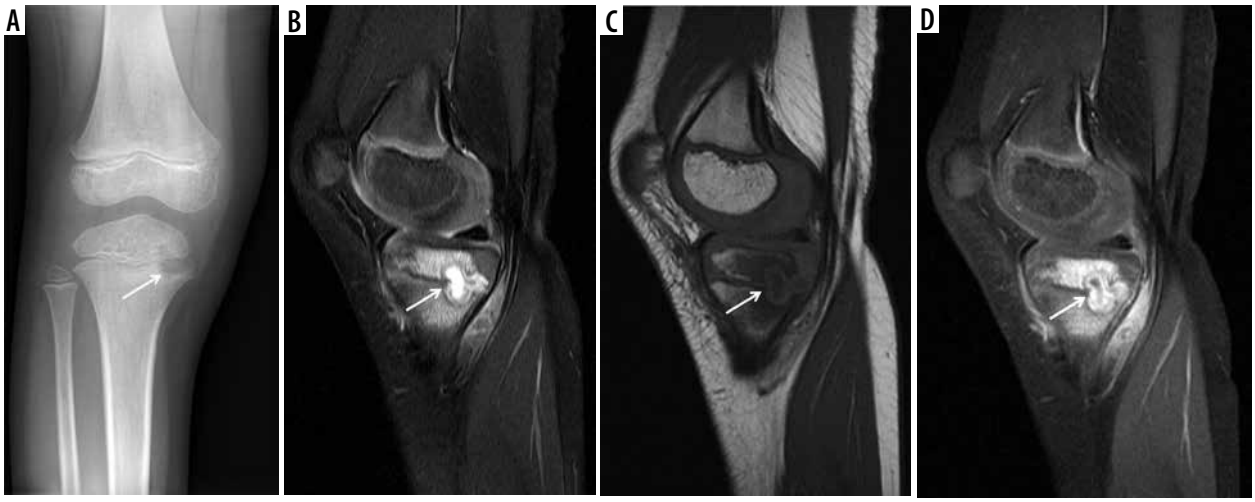

Figure 10. A 5-year-old male with Brodie abscess crossing the right proximal tibial physis. **A)** Internal oblique radiograph shows a circumscribed destructive osteolytic lesion at the medial aspect of the proximal tibial metaphysis involving the unfused physis and extending into the adjacent epiphysis with associated thin rim of reactive sclerosis (arrow). **B)** Sagittal proton density-weighted magnetic resonance (MR) image with fat saturation shows a lobulated lesion of high signal intensity lesion at the posteromedial aspect of the proximal tibial metaphysis with involvement of the physis and extension into the adjacent epiphysis with a tram-track-like rim of peripheral intermediate and central high signal consistent with brodie abscess (arrow) with adjacent high signal intensity bone marrow oedema. Note heterogeneous increased signal in the adjacent posterior soft tissues. **C)** On the sagittal T1-weighted MR image note decreased signal intensity in the affected bony structures with higher intermediate signal rim at the periphery of Brodie abscess consistent with hyperaemic phlegmonous tissue known as penumbra sign (arrow) with overlying thin linear low signal intensity consistent with reactive sclerosis. The affected posterior soft tissues show heterogeneous signal. **D)** Sagittal T1-weighted MR image with fat saturation post intravenous gadolinium-based contrast shows rim enhancing abscess cavity with central non-enhancement. Note surrounding linear low signal intensity related to reactive sclerosis. Also note enhancement of the surrounding bone marrow oedema, posterior periosteum, and adjacent posterior soft tissues

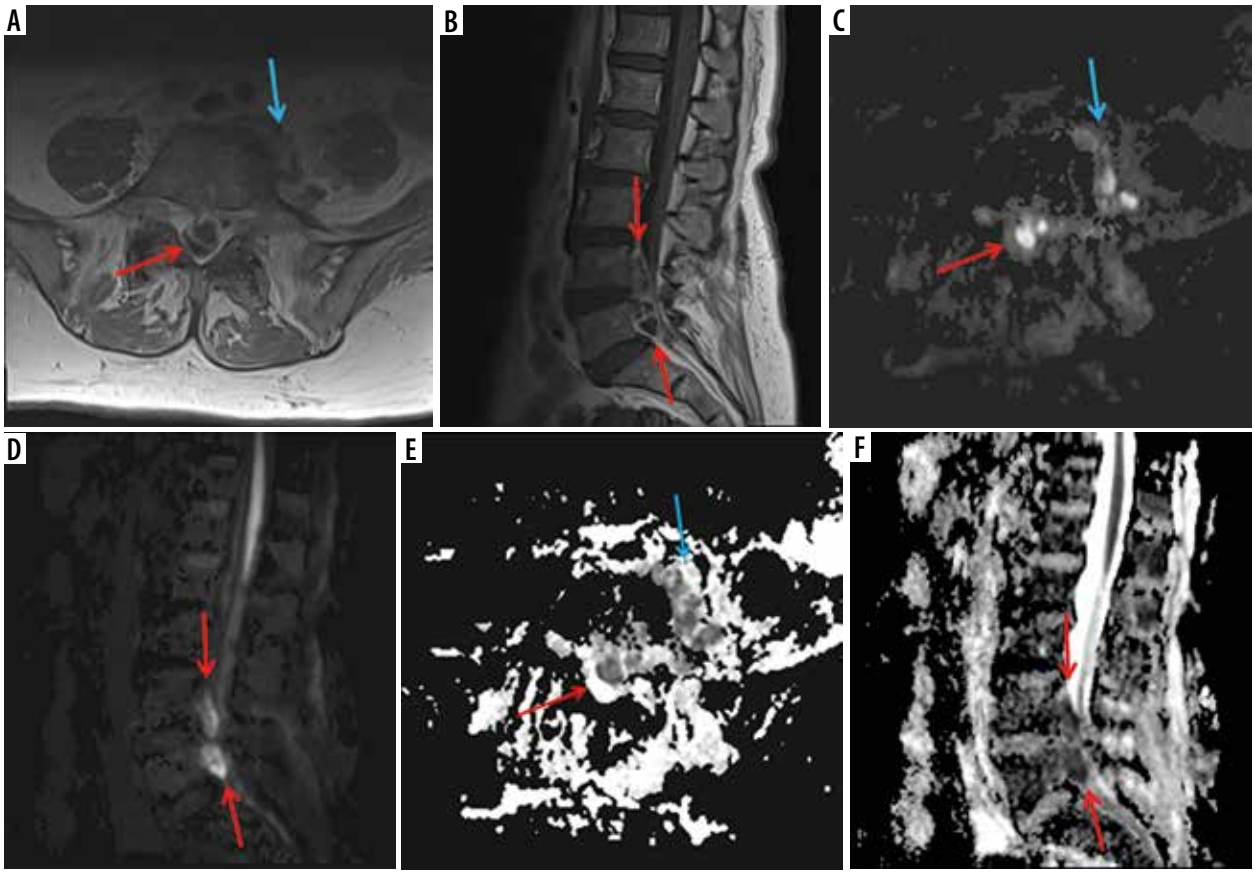

Figure 11. A 66-year-old female with *Bacteroides fragilis* L4-L5 discitis/osteomyelitis associated with epidural and prevertebral abscesses. Axial **(A)** and sagittal **(B)** T1-weighted magnetic resonance images post intravenous administration of gadolinium-based contrast show rim enhancing epidural (red arrows) and left prevertebral (blue arrow) soft-tissue abscesses. The epidural (red arrows) and left prevertebral (blue arrow) soft-tissue abscesses show high signal intensity on axial **(C)** and sagittal **(D)** diffusion-weighted imaging trace images and low signal intensity consistent with restricted diffusion on axial **(E)** and sagittal **(F)** ADC maps

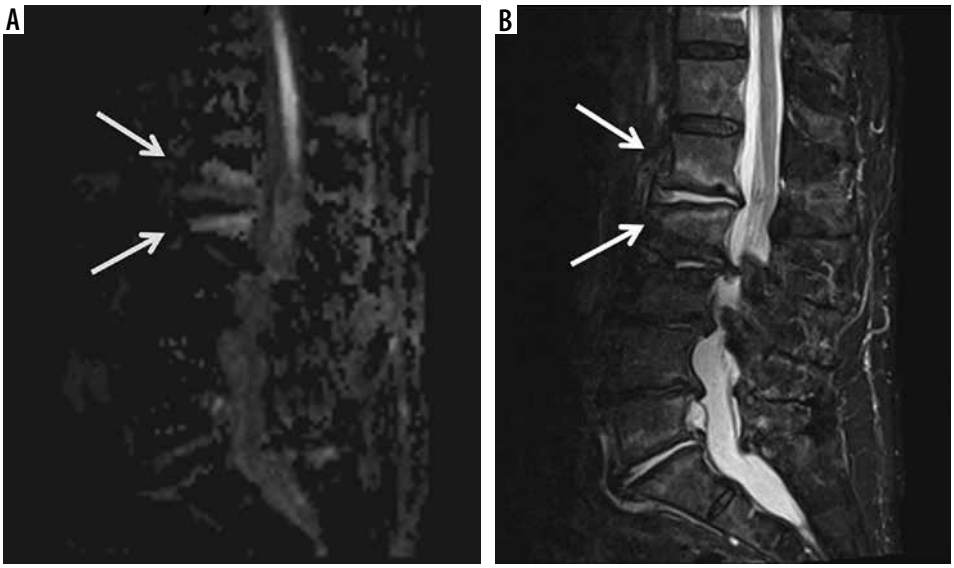

Figure 12. A 90-year-old male with severe back pain without fever, with positive diffusion-weighted imaging (DWI) "claw sign" compatible with Modic type I degenerative changes at L1-L2. Sagittal diffusion **(A)** and STIR **(B)** magnetic resonance images show well-marginated, linear regions of high signal at the L1-L2 level situated within the adjacent vertebral bodies at the interface of normal with abnormal marrow consistent with DWI "claw sign" associated with Modic type I degenerative changes

Figure 13. A 62-year-old male with group B *Streptococcus* L3-L4 and L5-S1 discitis-osteomyelitis and lack of diffusion-weighted imaging (DWI) "claw sign". Sagittal STIR **(A)** magnetic resonance (MR) image shows diffuse high signal intensity at the L3-L4 level involving the near entire vertebral bodies with marked disc space narrowing (arrows). At the L5-S1 level, note similar but less extensive diffuse high signal intensity of the L5 and S1 vertebral bodies (arrows) with more intense high signal intensity at the disc space eroding into the adjacent central vertebral body endplates (arrowheads). T1-weighted sagittal **(B)** MR image with fat saturation post intravenous administration of gadolinium-based contrast shows diffuse bone marrow enhancement of the affected vertebral bodies at both levels (arrows) with non-enhancement of the L5-S1 disc space consistent with discitis-osteomyelitis and most extensive enhancement at the central aspect of the opposing vertebral body endplates (arrowheads), possibly representing phlegmons. Sagittal diffusion **(C)** and ADC map **(D)** MR images show high signal intensity in the affected vertebral bodies and disc spaces (arrows) without DWI "claw sign"

Figure 14. A 22-year-old male with *Streptococcus anginosus* L1-L2 discitis-osteomyelitis and diffusion-restricted intradiscal abscess. Sagittal STIR **(A)** magnetic resonance (MR) image shows mild increased signal of the L1 and L2 vertebral bodies with an irregular high signal intensity intradiscal abscess (arrow) eroding into the adjacent vertebral body endplates. Sagittal T1-weighted MR image with fat saturation post gadolinium-based intravenous contrast shows marked enhancement of the L1 and L2 vertebral bodies with non-enhancing intradiscal abscess (arrow). Sagittal diffusion **(C)** image demonstrates high signal intensity within the intradiscal abscess (arrow). Sagittal ADC map **(D)** shows low signal intensity of the intradiscal abscess consistent with restricted diffusion (arrow)

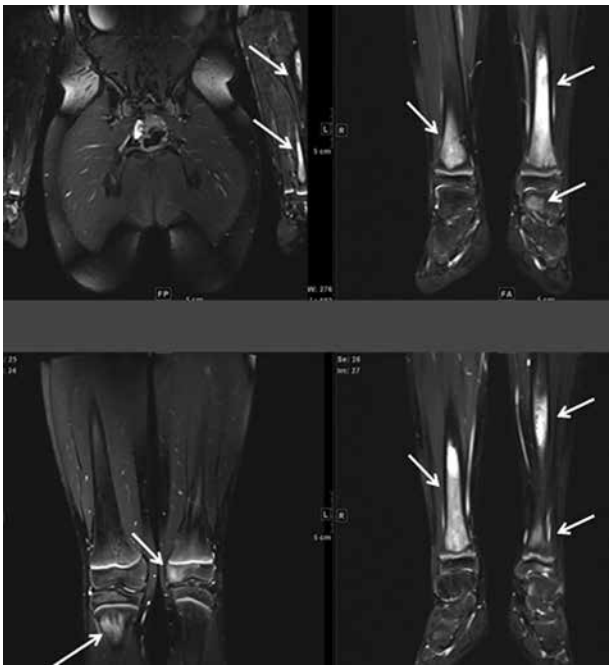

Figure 15. A 12-year-old male with chronic recurrent multifocal osteomyelitis (CRMO) presented with 2 weeks of persistent fever and bilateral lower extremity and left upper extremity pain. Selected coronal STIR images from whole-body magnetic resonance imaging show high signal intensity involving multiple bones including the bilateral tibiae, left talus, left medial femoral condyle, left humerus and left radius (arrows) consistent with CRMO. Courtesy of Kelley Marchall MD, Atlanta, Georgia

Figure 16. A 59-year-old male with infected total knee arthroplasty. **A)** Anteroposterior radiograph of the right knee shows soft-tissue thickening at the medial aspect of the right proximal leg (arrows) extending to the subjacent tibia. Note cortical irregularity and periostitis at the medial aspect of the proximal tibial diametaphysis (arrowheads), consistent with osteomyelitis. **B)** Coronal STIR magnetic resonance (MR) image shows heterogeneous high signal intensity soft tissue oedema at the medial aspect of the proximal leg (arrows) most extensive adjacent to the proximal tibia with subjacent cortical irregularity and periostitis consistent with osteomyelitis (arrowheads). **C)** Coronal T1-weighted MR image shows decreased intermediate signal intensity in the affected proximal medial leg soft tissues (arrows) with cortical irregularity, indistinctness, and periostitis of intermediate signal intensity along the proximal medial tibial diametaphysis (arrowheads). **D)** On the T1-weighted coronal MR image post intravenous administration of gadolinium-based contrast note non-enhancing soft tissue abscess (arrows) with enhancing surrounding phlegmonous tissues extending to the subjacent proximal tibia, which shows cortical indistinctness and enhancement consistent with osteomyelitis

neous enhancement. MRI can detect soft tissue or intraosseous gas but has lower sensitivity compared to CT [1, 6]. If present, gas bubbles appear as small focal signal voids on all MRI sequences.

MRI is also useful in guiding clinical treatment decisions based on the imaging findings combined with clinical severity of disease. It is also frequently used to monitor response to therapy. If pain, fever, or elevated inflammatory markers persist despite therapy, repeat imaging can be performed to exclude treatment failure [7]. However, findings such as bone marrow oedema as well enhancement may persist or worsen during treatment [7, 8]. Additionally, if surgical intervention was performed, post-operative changes may mimic ongoing infection.

Technical considerations

Although technical factors will vary with the MRI system being utilized (open versus closed bore, low versus high field strength, and coil technology) as well as the anatomic part to be imaged, imaging protocols typically consist of T1-weighted (T1W) and fluid-sensitive sequences, either T2-weighted images with fat saturation (T2W FS), proton density-weighted images with fat saturation (PDW FS), or short tau inversion recovery (STIR) images, obtained in at least 2 planes. Isotropic thin-cut 3D sequences enable subsequent reformatting in other imaging planes. STIR sequences are less susceptible to magnetic field inhomogeneity and are highly sensitive in detecting oedema and

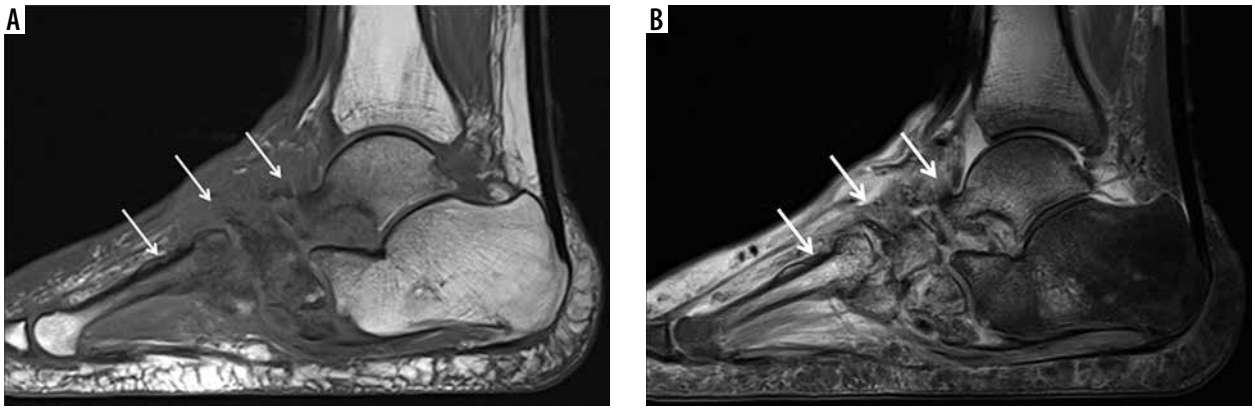

Figure 17. A 62-year-old male with insulin-dependent type II diabetes mellitus and right foot swelling without associated ulcer and no fever or laboratory findings suggestive of infection. **A)** Sagittal T1-weighted magnetic resonance (MR) image shows destructive changes and marked decreased signal intensity involving the entire midfoot, talar head and neck, part of the anterior process of the calcaneus, and the majority of the visualized metatarsal bone (arrows). **B)** Sagittal proton density-weighted MR image with fat saturation shows heterogeneous increased signal intensity in the affected bones with overlying soft tissue oedema, which is in conjunction with clinical and laboratory findings most consistent with Charcot arthropathy

fluid collections. T2W gradient-echo sequence and other gradient echo sequences exaggerate susceptibility artifacts and are helpful in the detection of soft-tissue or intraosseous gas and foreign bodies [1]. Coil selection will depend on the body part to be imaged, with dedicated surface or closed coils preferred. T1W images are obtained before and after the intravenous administration of contrast and are often obtained with fat saturation to improve visualization of contrast enhancement. Subtraction images may help in determining the degree of enhancement. Dynamic contrast-enhanced (DCE) MRI, as well as diffusion-weighted imaging (DWI), can provide additional evaluation of active infection. In DCE MRI, T1W acquisitions are repeated several times following the intravenous injection of gadolinium-based contrast to assess the dynamics of enhancement. While DWI is often helpful in evaluating MSK infections, if the area of interest is very small, it can be difficult to perceive restricted diffusion, which can limit the utility of DWI in some cases.

Radiographs should be routinely obtained prior to MRI for bone and soft-tissue infections, especially in a patient with a diabetic foot infection [6]. Radiographs are helpful to evaluate hardware, as well as for foreign bodies, soft tissue gas, and concurrent traumatic and pathologic findings (Figures 4A, 7A, 9A, 10A, 16A, 17A). Other imaging modalities also play an important role in the imaging of MSK infections. Ultrasound (US) is useful in the evaluation of soft-tissue infections, but it has limited use in the evaluation of osteomyelitis. Subperiosteal abscesses can be diagnosed by US. Computed tomography (CT) is useful in identifying soft-tissue gas and soft-tissue fluid collections. CT can show bone destruction, periostitis, and sequestration associated with osteomyelitis. Nuclear imaging is useful in the evaluation of multifocal infections. Technetium-99m methylene diphosphonate (Tc-99m MDP) bone scintigraphy is helpful in evaluating osteomyelitis, and gallium-67-labelled leukocyte imaging can be used to evaluate spinal osteomyelitis. Both of these imaging studies lack the high contrast and spatial resolution of MRI, which can be improved with the addition of single photon emission tomography-computed tomography (SPECT-CT). Three-phase Tc-99m MDP bone scintigraphy consisting of blood flow, blood pool, and delayed-phase imaging is typically performed over the region of interest, with delayed imaging of the entire skeleton obtained to evaluate for multifocal infection. Indium-111-labelled leukocyte scan combined with Technetium-99m sulphur colloid bone marrow imaging is useful in evaluating prosthetic joint infection. Fluorodeoxyglucose (FDG) positron emission tomography (PET) CT is also very useful in the evaluation of MSK infections, with reported sensitivities of greater than 95% and specificities of 75-99% [9]; however, FDG PET CT is limited in availability, is costly, and uses ionizing radiation.

US, CT, and fluoroscopy can provide image guidance for procedures such as joint arthrocentesis, bone biopsy, and abscess drainage to obtain tissue and fluid samples in cases of suspected soft tissue or bone infections. Culture of these specimens can guide antibiotic therapy. Image-guided drain placement can also be considered.

Pathophysiology of musculoskeletal infections

Soft-tissue infections often result from direct inoculation through broken skin, either from trauma, prior surgery, or a diabetic ulcer, with haematogenous seeding less common. Osteomyelitis and septic bursitis commonly result from haematogenous seeding in children, and as a result of either contiguous spread of concurrent infection or direct inoculation from trauma in the appendicular skeleton in adults. Infections of the axial skeleton in adults, particularly those in the spine, most commonly result from hematogenous seeding. Septic arthritis is most commonly caused by hematogenous seeding in both children and adults. Soft-tissue and bone infections may occur in both children and adults in the postoperative and postprocedural state, secondary to either direct inoculation during

Figure 18. A 40-year-old male with insulin-dependent diabetes mellitus, methicillin-resistant *Staphylococcus aureus* infection, and draining deep soft ulcer at the distal aspect of the great toe with associated MRSA soft-tissue infection of the great toe with osteomyelitis involving the phalanges and septic interphalangeal joint. **A)** Anteroposterior radiograph shows destructive changes and fragmentation of the great toe phalanges (arrows) with overlying soft tissue oedema and irregularity. Note associated scattered foci of soft tissue gas extending into the great toe interphalangeal joint and along the distal first metatarsal (arrowheads). **B)** Sagittal STIR magnetic resonance (MR) image shows a deep plantar soft-tissue ulcer along the distal aspect of the great toe extending to the interphalangeal joint (arrowhead). There is diffuse increased signal intensity involving the great toe phalanges (arrows). Note extensive high signal intensity soft tissue oedema more pronounced along the plantar aspect of the great toe. **C)** Axial T1-weighted MR image shows deep soft tissue ulcer at the distal aspect of the great toe (arrowhead) and marked destructive changes of the great toe phalanges with foci of low signal intensity bone marrow effacement (arrow). **D)** Axial T1-weighted MR image with fat saturation post intravenous gadolinium-based contrast shows marked enhancement of the affected great toe phalanges (arrow) and markedly enhancing overlying soft tissue oedema with scattered small rim enhancing fluid collections consistent with abscesses as well as a small amount of draining fluid at the base of the soft-tissue ulcer (arrowheads)

surgery or a procedure, or from contiguous spread from a postoperative wound/incision.

While many infections are polymicrobial, *Staphylococcus aureus* is the most common causative organism in all age groups. In neonates, *Staphylococcus aureus, Streptococcus,* and *Escherichia coli* are common causative organisms. In children between 1 and 3 years of age, *Staphylococcus aureus, Streptococcus pyogenes,* and *Haemophilus influenzae* are the leading causative organisms, while in children older than 4 years of age, *Staphylococcus aureus* is a common causative agent, and infections are predominantly from hematogenous seeding. In adults, *Staphylococcus aureus* and enteric species are the most common causative organisms. Some patients may be susceptible to MSK infections from unusual organisms. For example, patients with sickle cell disease classically suffer from *Salmonella*-related infections, even though *Staphylococcus aureus* is still the most common causative organism. In patients with intravenous drug use, *Pseudomonas* and *Klebsiella* are common infectious organisms. Approximately 1-3% of all tuberculosis (TB) cases involve the MSK system, and spinal involvement accounts for 50% of these cases [10-12]. The knee and the hip are the most commonly affected appendicular joints, while the bones of the lower extremity are most commonly involved in TB osteomyelitis [10-12]. Fungal MSK infections most commonly occur in immu-

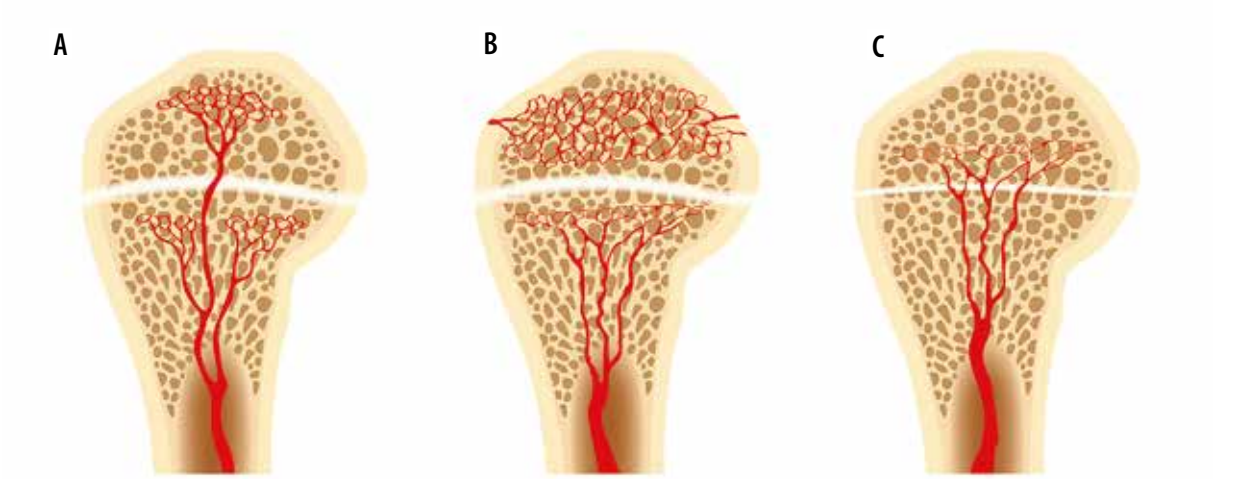

Figure 19. An artist's drawing of the end of the long bone blood supply **(A)** in an infant with the metaphyseal vessels crossing the open physis and extending into the epiphysis, **B)** child (1-16 years old) without extension of the metaphyseal vessels through the open physis into the epiphysis, and **(C)** adult with metaphyseal vessels extending through the closed physis into the epiphysis

Figure 20. Cellulitis of the left gluteal region in a 36-year-old female patient. Gluteal region photograph shows redness of the skin consistent with cellulitis. Courtesy of Jordan Smith MD, Tuscon, Arizona

Figure 21. Necrotizing fasciitis of the lower leg in a 40-year-old male patient. Lower leg photograph shows marked discoloration of the skin with an area of necrosis (arrows). Courtesy of Jordan Smith, Tuscon, Arizona

nocompromised patients, and vary from rapidly destructive to indolent in behaviour [13].

In young children (less than 1 year of age), there is direct vascular communication between the epiphysis and the metaphysis, allowing extension of infection into the epiphysis, and eventually the joint, with resulting septic arthritis [14-17] (Figures 10, 19). These vessels involute in early childhood (usually by 2 years of age), but the metaphyses of several long bones, in particular the proximal humerus, proximal radius, proximal femur, and distal fibula, remain intraarticular [15, 18, 19]. Osteomyelitis in these areas in children with adjacent joint effusions should be evaluated for septic arthritis [15, 19]. Additionally, transepiphyseal extension of pyogenic osteomyelitis has been shown to occur more commonly in children [17]. In adults, hematogenous osteomyelitis most commonly occurs in the metaphysis due to slow flow in terminal capillaries at the junction of the metaphysis and the physis [14, 20].

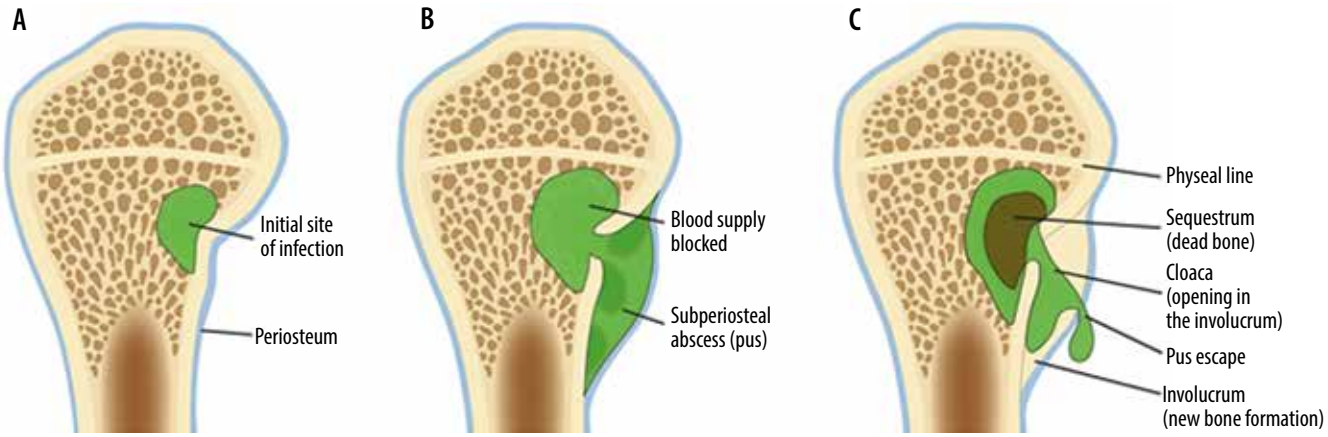

Figure 22. An artist's drawing of osteomyelitis progression, subacute to chronic. **A)** Initial site of osteomyelitis involving the medial aspect of the long bone metaphysis/intraosseous abscess (green). **B)** The abscess extends through the cortex into the subperiosteal space forming subperiosteal abscess (shades of green). **C)** Chronic osteomyelitis with a detached central necrotic bone fragment/sequestrum (brown) within the intraosseous abscess (green) with peripheral new bone formation/involucrum and a cortical and periosteal opening in the involucrum/cloaca allowing pus to escape

Musculoskeletal soft-tissue infections

MSK soft-tissue infections include cellulitis (Figures 1, 2, 4B-D, 7, 8A, 8C, 9, 20], abscess/phlegmon (Figures 1, 2, 3C-D, 11, 13B, 14, 16D, and 18D), superficial and deep fasciitis including life-threatening necrotizing fasciitis (Figures 3, 4, 21), pyomyositis (Figures 2 and 3), infectious/septic bursitis (Figure 6), and tenosynovitis (Figure 7E-G], and infectious lymphadenitis (Figure 13D). These conditions have characteristic MRI findings that need to be correlated with clinical symptoms, physical examination findings, and laboratory values. MSK soft tissue infections are sometimes difficult to differentiate from inflammatory non-infectious diseases, such as various rheumatologic and post-traumatic conditions. The presence of rim-enhancing soft-tissue abscesses facilitates the diagnosis of an infectious rather than an inflammatory process. Of importance, MSK soft-tissue infections may be complicated by compartment syndrome, a serious condition that threatens tissue viability and requires prompt surgical treatment.

Clinical and magnetic resonance imaging findings of musculoskeletal soft-tissue infections

Cellulitis

Cellulitis is an infection of the deep dermis and superficial subcutaneous tissues, and is typically of bacterial aetiology [1, 21-25]. The superficial fascial planes are commonly affected. Associated skin and soft tissue ulcerations may be present. The most common organisms are *Staphylococcus aureus* and *Streptococcus pyogenes* [26]. Cellulitis most often occurs from direct inoculation.

Cellulitis is most often a clinical diagnosis, because soft tissue oedema may result from trauma, lymphoedema, venous stasis, and cardiac insufficiency. MRI may be obtained to evaluate for associated abscesses or deep soft-tissue extension, involvement of the adjacent joint, or osteomyelitis [26-28]. MRI will show thickening of the skin and subcutaneous fat, with hypointense signal on T1W images and hyperintense signal on fluid-sensitive images, and variable enhancement following intravenous contrast administration (Figures 1, 2, 4B-D, 7, 8A, 8C, 9, 20] [1, 24-26, 28-31]. Cellulitis may show restricted diffusion on DWI sequences (Figures 2D-E) [32]. Ulcerations may be seen on MRI as defects on the skin surface, with variable degrees of communication with the deeper soft tissue and bone, and are usually hyperintense on fluid-sensitive images, with peripheral enhancement following intravenous contrast (Figures 17B-D) [31, 33, 34].

Cellulitis is treated with antibiotics and debridement as needed. Wound care is needed for ulcerations.

Abscess/phlegmon

An abscess is a focal fluid collection containing inflammatory cells, bacteria, and necrotic tissue debris surrounded by hypervascular, inflamed connective tissue [1, 25]. A phlegmon is defined as enhancing infected granulation tissue, frequently surrounding an abscess. An abscess may be located in either the superficial or the deep soft tissues and may occur secondarily to direct inoculation, a pre-existing foreign body, contiguous spread from an adjacent infection, or from hematogenous spread [1-3, 35-37].

On MRI, an abscess will have increased signal on fluid sensitive sequences, decreased signal on T1W images, and will show peripheral enhancement following intravenous contrast administration (Figures 1, 2, 3, 11, 13B, 14, 16D, 18D]. Gas within an abscess will be seen as low signal on all sequences with a susceptibility artifact that is exaggerated on gradient echo sequences. Abscesses are often surrounded by hyperaemic phlegmonous tissue, which will be increased in signal on fluid-sensitive sequences and show enhancement on the post-contrast sequences (Figures 2C,

16D). The "penumbra sign", or the presence of a thin rim of hyperintense signal along the periphery of the abscess, on T1W images has been described to help differentiate soft tissue abscesses from necrotic tumours (Figure 2B) [38].

On DWI, purulent material with an abscess will restrict the free diffusion of water molecules, resulting in high diffusion signal on fractional anisotropy/trace images and low apparent diffusion coefficient (ADC) map signal intensity, which is particularly useful in patients who cannot receive gadolinium-based contrast agents due to impaired renal function or contrast allergy (Figures 2D-E, 11C-D] [25, 39-42]. Use of DCE MRI to differentiate viable tissue, which enhances, from necrotic tissue, which does not enhance, has been described [41].

Treatment for abscess is dependent on size and location, and includes percutaneous drainage, surgical debridement, and intravenous and oral antibiotics.

Myositis/pyomyositis

Myositis is a non-specific term for muscular inflammation, the aetiology of which may be an infectious process. Pyomyositis is a bacterial infection of skeletal muscle, which leads to muscle oedema and often phlegmon formation followed by abscess formation [1, 26, 43, 44]. Previously seen mainly in tropical climates, pyomyositis is increasing in frequency in temperate climates [44-46]. Trauma is the leading cause (25-40%) of pyomyositis in temperate climates, although haematological seeding from adjacent infection is also possible [44, 46, 47]. Pre-existing muscular injury (muscle trauma such as haematoma, underlying myositis, strenuous physical activity) can predispose to pyomyositis [26, 44, 46-49].

On MRI, pyomyositis will demonstrate muscular oedema and enlargement, with increased signal on fluid sensitive sequences and variable enhancement on the post-contrast sequences (Figures 2 and 3). Phlegmon and abscesses may be present. Adjacent bones and joints should be scrutinized for osteomyelitis and septic arthritis, respectively. DWI of the abscess cavity will show restricted diffusion centrally; however, there is often increased diffusion in the surrounding muscle due to inflammation and expanded extracellular space (Figures 2D-E) [32]. Treatment for pyomyositis is dependent on size and location, and includes percutaneous drainage, surgical debridement, and intravenous antibiotics [44].

Diabetic myonecrosis is a non-infectious process that may mimic pyomyositis [1, 24, 26, 36]. Patients often have a long-standing history of uncontrolled diabetes and may develop muscular infarcts that often involve entire muscles and may be bilateral [1, 24, 50, 51]. Diabetic myonecrosis is more common in the lower extremities, particularly involving the quadriceps and the anterior thigh muscles [23, 24, 26] MRI will show subcutaneous, perifascial and muscular oedema as well as perifascial fluid of high signal on fluid sensitive sequences, and rim-enhancing areas of intramuscular non-enhancement in the regions of infarcts on the post-contrast sequences (Figure 5) [23, 24, 26, 29, 51, 52]. Diabetic myonecrosis can be distinguished from abscess by the clinical presentation, and patients with diabetic myonecrosis should not have an elevated white blood cell count nor elevated inflammatory markers; however, diabetic myonecrosis can be complicated with superinfection. Diabetic myonecrosis without associated infection is treated with medical management.

Superficial, deep, and necrotizing fasciitis

In infectious fasciitis, both the superficial and the deep fascia may be infected, and the cause of infection is usually direct inoculation from trauma. Necrotizing fasciitis is a severe, rapidly progressive, potentially fatal subtype of infectious fasciitis that typically occurs in immunocompromised patients (Figure 21) [22, 23, 26, 28, 29, 53-57]. Most infections are polymicrobial, often with *Clostridium* species and gram-positive cocci [2, 26, 28, 29, 54, 58]. The lower extremities are involved in 50% of cases [25, 56]. Necrotizing fasciitis may be secondary to direct inoculation or may arise secondarily to direct spread from a perforated viscus or urogenital organ [59]. The resulting tissue ischaemia and liquefactive necrosis may spread rapidly, up to an inch per hour [59]. The overall morbidity and mortality rate is 30-80% [24, 29, 54, 56].

In infectious fasciitis, on MRI the affected fascia will be thickened, with increased signal on fluid sensitive sequences and variable enhancement following intravenous contrast administration (Figures 3A-C, 4B-D] [1, 36, 60, 61].

Patients suspected of having necrotizing fasciitis should undergo immediate surgical evaluation rather than imaging (Figure 21). Radiographs and computed tomography (CT) examinations are less time-intensive than MRI and will readily demonstrate soft-tissue gas (Figure 4A). On MRI, there is dermal and soft tissue thickening, with reticulated increased signal intensity on fluid-sensitive sequences and variable signal intensity on T1W images along the deep fascial planes, which are often thickened and show heterogeneous enhancement following intravenous contrast administration; gas is variably present, and the absence of gas does not exclude the diagnosis (Figures 4B-D) [1, 24, 25, 29, 53, 54, 56, 59]. The lack of contrast enhancement may be due to hypoperfusion and tissue necrosis, which may underestimate the disease extent. Subcutaneous oedema may be present but is less common than in cellulitis [29]. In the early stages, the muscles are spared [53, 55]. Kim *et al.* showed that patients with necrotizing fasciitis have ≥ 3 mm of thick fascial oedema on T2W FS images, extensive involvement of the deep fascia (often with low signal intensity on T2W FS images and areas of non-enhancement), and involvement of 3 or more compartments in 1 extremity when compared to patients with non-necrotizing fasciitis [22, 23, 26, 28, 57, 58, 62].

The differential diagnosis includes other forms of non-infectious fasciitis including paraneoplastic, eosinophilic, and nodular fasciitis [29], and venous obstruction. Distinguishing infectious from non-infectious fasciitis is based mainly on distribution and clinical presentation [29].

Superficial fasciitis often occurs with cellulitis and is treated with antibiotics. Deep fasciitis also may be treated with antibiotics, and surgical intervention is reserved for unresponsive cases [1]. Necrotizing fasciitis is a surgical emergency and is treated with prompt debridement, fasciotomy, and antibiotics [1, 2, 24, 36, 53, 54, 59]. Skin grafting and hyperbaric oxygen therapy are occasionally needed [2, 59].

Acute compartment syndrome results from a prolonged increase in intramuscular pressure with decreased arterial pressure, often affecting the anterior and lateral compartments of the leg, and it usually occurs secondary to prolonged ischaemia, fractures, and crush injuries [24, 29]. When intramuscular pressures increase above 15- 20 mmHg, capillary perfusion and lymphatic flow are impaired, resulting in ischaemic muscular injury [24]. Interstitial oedema from capillary leakage also results in decreased muscle perfusion [24]. An interstitial tissue pressure of 30 mmHg is the typical threshold at which the diagnosis of compartment syndrome should be considered [1, 29].

On MRI, there is low muscular signal on T1-weighted images and a diffuse increase in muscular signal intensity on fluid-sensitive images, with variable contrast enhancement [24, 29]. Treatment of acute compartment syndrome is fasciotomy and decompression [24, 29].

Infectious bursitis

Bursitis is most often non-septic, and it is often caused by repetitive trauma, crystal deposition, and inflammatory arthropathies [26, 63, 64]. Infectious bursitis is most commonly due to bacterial organisms, but may be due to fungal, tuberculous, or atypical mycobacterial aetiologies. Septic bursitis may occur due to either direct inoculation or spread from an adjacent infection, such as a pre-existing inflamed bursa; haematogenous spread is much less common [26, 63, 65, 66]. Superficial septic bursitis is more common than deep septic bursitis [66]. The olecranon and prepatellar bursae are most commonly affected, and approximately one third of olecranon and prepatellar bursitis are septic [1, 26, 63-66]. Iatrogenic septic bursitis can be caused by attempted aspiration or injection of a non-infected bursa [66].

On MRI, infectious bursitis should be considered when the bursa is distended with either fluid, which may be simple or complex, and/or enhancing synovitis (Figure 6). Simple fluid is hypointense in signal on T1W images and hyperintense signal on fluid sensitive images, and demonstrates smooth, thin peripheral synovial enhancement following intravenous contrast administration. If the fluid is complex, due to the presence of blood or debris, it will have a more heterogeneous appearance. Active infectious or inflammatory synovitis will show thick enhancement on post-contrast sequences. If foci of internal low signal are present, the presence of gas should be considered. The peribursal soft tissues may be oedematous, and overlying cellulitis is often present [1]. There may be a sympathetic effusion in an adjacent joint [65]. Septic bursitis may show restricted diffusion on DWI [32].

Superficial infectious bursitis is usually treated with antibiotics, often empirically to avoid iatrogenic infection from aspiration [67]. Percutaneous drainage and surgical bursectomy are reserved for extremely distended bursae and refractory cases that do not respond to antibiotic therapy [1, 65, 68].

Infectious tenosynovitis

Infectious tenosynovitis usually occurs from direct inoculation from penetrating trauma or from extension of adjacent infection [1, 26, 68, 69]. This is most frequently due to bacterial infection but may also be secondary to fungal, tuberculous, and atypical mycobacterial aetiologies [1, 26, 69]. Retained foreign bodies may complicate tenosynovitis [69]. Tendon necrosis may occur in the absence of appropriate treatment [69]. Infectious tenosynovitis is important to detect because it may allow rapid migration of organisms from one anatomic region to another.

On MRI, infectious tenosynovitis should be considered when the tendon sheath is distended with simple or complex fluid collections, accompanied by variable thickness and irregular synovial enhancement, frequently with adjacent cellulitis (Figures 7E-G). If foci of diffusely low signal are present, the presence of gas should be considered. The adjacent tendon may become thickened and have an indistinct signal [1, 31-34]. DWI may show restricted diffusion in infectious tenosynovitis [32]. Clinical history and laboratory values can help differentiate septic tenosynovitis from inflammatory tenosynovitis.

In the hand, pyogenic tenosynovitis of the flexor tendons is a particularly challenging closed-space infection given the complex anatomy of the ulnar and radial bursae. The radial bursa is in continuity with the flexor pollicis longus tendon sheath, and the ulnar bursa frequently communicates with the little- or ring-finger flexor tendon sheaths. The index- and middle-finger tendon sheaths typically do not communicate with these bursae. The variability in bursal and tendon sheath interconnections in the hand and the space of Parona, located between the fascia of the pronator quadratus muscle and the flexor digitorum profundus tendons in continuity with the carpal tunnel, allows for rapid spread of infection [70].

Early infectious tenosynovitis is often managed with antibiotics and elevation, with surgical decompression often necessary if there is no improvement within 24 hours [1, 68, 71].

Infectious lymphadenitis

Infectious lymphadenitis is inflammation of the lymphatic system, often caused by a bacterial infection, or less likely a parasitic or mycobacterial infection [72]. Gram-positive bacilli such as group A streptococci are the frequent causative organisms [72, 73].

MRI will show enlarged lymph nodes, often with adjacent soft tissue oedema (Figure 3D) [74]. Acute bacterial lymphadenitis is typically treated with antibiotics.

Musculoskeletal bone infections

MSK bone infections include osteomyelitis (Figures 6, 7, 8, 9, 13, 14, 16, 22) and septic arthritis (Figures 6, 7, 18).

Clinical and magnetic resonance imaging findings of musculoskeletal bone infections

Osteomyelitis: acute, subacute, and chronic

Osteomyelitis is infection of the bone marrow, which may occur due to haematogenous dissemination from a distant site, by direct inoculation from trauma, or via spread from an adjacent soft tissue infection; the most common causative agent is *Staphylococcus aureus* [20, 30]. Haematogenous osteomyelitis is more common in children [20]. In adults, haematogenous osteomyelitis occurs more commonly within the spine, pelvis, and small bones, and is often secondary to bacteraemia from endocarditis, genitourinary infections, gastrointestinal infections, or intravenous drug use [75, 76]. Direct inoculation is usually secondary to penetrating trauma or open fracture.

Osteomyelitis may be acute, subacute, or chronic (Figures 6, 7, 8, 9, 13, 14, 16, 22). In the acute phase, there is osseous hyperaemia and oedema, with resulting osseous demineralization, destruction of bony trabeculae, and replacement of the normal bone marrow fat with neutrophilic infiltrate [75]. Subperiosteal abscess formation can occur in the setting of osteomyelitis, more commonly in children than in adults (Figures 8 and 22). Subperiosteal abscesses are thought to occur from outward extension of infection from the cortex or as a result of direct inoculation from trauma or surgery [77, 78].

MRI is highly sensitive and specific in the diagnosis of osteomyelitis. A systematic review by Llewellyn *et al.* showed that in adults, MRI had 95.6% sensitivity and 80.7% specificity for the diagnosis of osteomyelitis [79]. A recent meta-analysis by Llewellyn *et al.* showed MRI to have 96.4% sensitivity and 83.8% specificity for the detection of osteomyelitis in people with diabetic foot ulcers [80]. On MRI, acute osteomyelitis is characterized by bone marrow and periosteal oedema, which shows high signal intensity on fluid-sensitive sequences, decreased/intermediate signal with bone marrow effacement on the T1W images, sometimes with interspersed foci of preserved marrow fat, and enhancement on the postcontrast sequences (Figures 6, 7B-G, 8, 9B-D, 13, 14, 16B-D, 18B-D]. Adjacent enhancing soft-tissue oedema is typically present. Intraosseous and subperiosteal abscess and areas of necrosis do not enhance (Figure 8) [14, 75]. On DWI, intraosseous and subperiosteal abscesses may show restricted diffusion [23, 32].

In subacute and chronic osteomyelitis, an intra-osseous abscess can form, with resulting necrosis of a portion of the bone, known as a Brodie abscess (Figures 9, 10, 22) [14, 76]. Brodie abscesses may be intramedullary or cortical. Cortical Brodie abscess is characterized with central necrosis in an area of cortical thickening while an intramedullary Brodie abscess is characterized by a necrotic centre surrounded by peripherally ill-defined sclerosis.

Chronic osteomyelitis, often defined as lasting more than 6 weeks, is manifested by osteonecrosis surrounded by persistent infection (Figures 9 and 22). The fragment of the infected necrotic bone, known as the sequestrum (Figures 9 and 22), develops after approximately 30 days and serves as a reservoir for bacteria. The sequestrum is most specific for chronic osteomyelitis and is separated from the living bone by granulation tissue, surrounded by reactive new bone formation, known as an involucrum (Figures 9 and 22). A periosteal defect/opening in the involucrum is known as a cloaca (Figures 9 and 22). The continuous sinus/fistulous tracts eventually extend to the skin surface [14, 30, 75, 76]. Malignant transformation within the draining sinus tract to squamous cell carcinoma can occur in longstanding chronic osteomyelitis with the reported incidence of less than 0.5% [14].

In subacute osteomyelitis, there may be a thick rim of vascularized granulation tissue along the periphery of the intraosseous abscess, with hyperintense signal on T1W images, known as the "penumbra" sign (Figure 10C) [14, 38, 81]. The penumbra sign has a specificity of 96% for the presence of infection with a sensitivity of 27% [14, 38, 81].

In chronic osteomyelitis, the sequestrum will be of low signal on all sequences, with surrounding high signal granulation tissue on fluid-sensitive sequences, which may eventually become low signal on all sequences due to the formation of avascular, necrotic tissue (Figures 9B-D) [75, 76]. The surrounding involucrum and thickened periosteum have low signal on all sequences (Figures 9B-D). The cloaca will be an intermediate to high signal tract from the sequestrum through the involucrum on fluid-sensitive images (Figure 9B-D). Sinus tracts may be present from the skin surface to the infected bone. The walls of the sinus tract will enhance. Infected bone will enhance; necrotic bone will not enhance. The treatment of chronic osteomyelitis is often surgical, with resection of the sequestrum, debridement of infected bone, and intravenous antibiotics [14].

In the adult spine, osteomyelitis typically occurs in the vertebral body endplate from hematogenous spread

and extends into the disc and eventually the contralateral vertebral body endplate; in the paediatric patient, infection tends to originate in the disc, because it is more vascularized [30, 40]. MRI findings are dependent on the causative agent, but initially include loss of the vertebral body hypointense cortex on both T1W and fluid-sensitive images [40]. Additional MRI findings include bone marrow oedema signal on fluid-sensitive images, fatty marrow effacement with low signal on T1W images, and enhancement following contrast administration in the vertebral body endplate, with high signal oedema on fluid-sensitive images and enhancement in the disc (Figures 11, 13, 14) [30, 39, 40]. Epidural and paraspinous phlegmons and abscesses may form (Figures 11A-D) [39, 40]. DWI can help differentiate acute discitis-osteomyelitis from Modic I degenerative changes, which can look similar on MRI (Figures 11E-F, 12, 14C-D] [40, 82]. On sagittal DWI of the spine, a discrete edge of diffusion hyperintensity in the region of bone marrow oedema suggests Modic I changes ("claw sign") (Figure 12) [82]. Diffuse and ill-defined margins of diffusion hyperintensity within bone marrow oedema suggests discitis-osteomyelitis ("reverse claw sign") [40]. Adjacent psoas muscle infection also suggests discitis-osteomyelitis.

Chronic recurrent multifocal osteomyelitis (CRMO) is an inflammatory non-infectious autoimmune osteomyelitis that occurs more commonly in children (Figure 15) [75, 83]. Patients most often present with osteolytic lesions, periostitis, soft tissue oedema, and eventual osseous sclerosis [75]. Lesions are often bilateral and symmetrical [75]. Clavicular involvement is common; the metaphyses and epiphyses of the femur, tibia, and humerus are also frequently affected (Figure 15) [75, 83].

Septic arthritis

Septic arthritis is an infection of the joint which may occur from direct trauma, pre-existing hardware, operative intervention, and hematogenous spread. It most commonly affects the large joints that have a rich blood supply, such as the hip, shoulder, and knee [23, 25]. Septic arthritis occurs most frequently in individuals under 3 years old and over 55 years old [84]. An infectious aetiology should always be considered in patients with a monoarticular arthritis. Predisposing factors include underlying inflammatory arthropathy, prior trauma, recent surgical intervention, pre-existing hardware, use of immunosuppressive drugs, and underlying medical conditions such as diabetes mellitus and cirrhosis [15]. The gold standard for diagnosing septic arthritis is arthrocentesis with culture.

Bacterial arthritis may lead to rapid joint destruction with loss of function, within 24-48 hours of onset [15, 23, 69]. Delay in diagnosis may result in significant bone and cartilage destruction, osteonecrosis, secondary osteoarthritis, and eventual osseous ankylosis [85]. In children, septic arthritis can lead to premature or asymmetrical closure of the growth plate, with subsequent limb length discrepancy and angular deformities, which may require future surgical interventions [16].

Children with septic arthritis often have associated osteomyelitis and adjacent soft-tissue infections [15, 86-88]. Criteria established by Kocher *et al.* are useful in differentiating septic arthritis in children with an inflamed hip from other aetiologies such as transient synovitis [15, 88, 89]. They include non-weight bearing, temperature greater than 38.5°C, white blood cell count greater than 12,000 cells/mm^3, and erythrocyte sedimentation rate greater than 40 mm/hour. The presence of 1 criterion has a 3% probability, 2 criteria have a 40% probability, 3 criteria have a 93% probability, and 4 criteria have a 99% probability of septic hip.

On MRI, a septic joint will usually have joint effusion and thick enhancing synovitis (Figures 6, 7B-G, 18) [25, 90]. MRI findings of osteomyelitis often will be present in the adjacent bones, with high signal intensity bone marrow oedema present on fluid-sensitive images, low signal from effacement of the normal fatty marrow on T1W images, with marrow enhancement following the administration of intravenous gadolinium-based contrast (Figures 6, 7B-G, 18). Osseous erosions and bone destruction may be present (Figures 6 and 7) [85]. Cartilage loss is also possible, with defects best appreciated on the fluid-sensitive images. There may be inflammatory changes in the adjacent soft tissues, including subcutaneous, fascial, and muscular oedema without or with abscess formation, bursitis, and tenosynovitis (Figures 6, 7, 18) [30]. In a septic joint, the purulent and pus-like intra-articular fluid may show restricted diffusion on DWI [23, 32].

Treatment of septic arthritis includes antibiotics combined with joint irrigation and debridement.

Surgical hardware infections

Infection can occur as an early or a late complication of hardware placement. It may be secondary to direct contamination during surgery, haematogenous seeding, or from extension of an adjacent infection [91, 92]. *Cutibacterium propionicum* (formerly *Propionibacterium*) can be the causative infectious agent when hardware is present, and culture time must be prolonged to 14 days to exclude this organism. Radiographs are the preferred initial imaging modality for the evaluation of infected hardware and may show lucency along the bone-metal or bone-cement interface, cortical irregularity, periostitis, and soft tissue swelling (Figure 16A). Although susceptibility artifacts from hardware may obscure adjacent structures, newer MRI metal artifact-reduction techniques such as vendor-specific metal artifact-reduction sequences (MARS), slice encoding for metal artifact correction (SEMAC), and multi-acquisition with variable-resonance image combination (MAVRIC) have allowed greater use of MRI in the evaluation of hardware-associated infections [91, 93] (Table 1). More recently,

surgical hardware made of less ferromagnetic alloy materials may produce less artifacts [91]. MRI is useful in detecting osteomyelitis, joint, and perihardware fluid collections and sinus tracts (Figures 16B-D). On MRI, lamellated hyperintense synovitis has an 86 to 92% sensitivity and 85 to 87% specificity for infection of knee arthroplasties [93-95].

In the instrumented spine, infection usually results in discitis/osteomyelitis, with low T1W signal intensity, high fluid signal intensity, and contrast enhancement within the intervertebral space and adjacent vertebral marrow. Adjacent inflammatory and infectious changes such as enhancing paraspinal or epidural phlegmon or rim-enhancing abscess formation may occur (Figures 11, 13, 14) [96].

Management of hardware-associated infections is dependent on many factors, including timing of infection relative to surgery, as well as location and type of surgical implant. Treatment often requires removal of existing hardware, placement of local antibiotic impregnated cement or hardware, an adequate course of antibiotic therapy, and eventual hardware revision [97-99].

Diabetic foot infections

Diabetic foot infections are thought to be secondary to sensory, autonomic, and motor neuropathy as well as vascular and immune compromise [14, 41, 52, 75, 100]. Distinguishing diabetic foot infections from evolving Charcot arthropathy may be challenging because the clinical and imaging features overlap. Most cases of diabetic foot infections occur in the setting of direct extension from an overlying soft-tissue ulcer [31, 33, 34, 52, 100]. In these cases, osteomyelitis typically involves a weight-bearing bone subjacent to an ulcer, most commonly the calcaneus, fifth metatarsal, first metatarsal, and great toe distal phalanx [14, 52, 100]. In a neuropathic foot, altered biomechanics increase the prevalence of bone marrow signal alterations located within the midfoot [14, 41, 52]. In the non-infected neuropathic foot, the bone marrow signal changes on MRI tend to be articularly centred (Figure 17) [101]. Skin ulcers and bone marrow oedema occur in neuropathic feet with and without superimposed infection. The most useful MRI finding to differentiate osteomyelitis in a neuropathic foot from an uninfected neuropathic foot is the presence of a sinus tract from a skin ulceration to the affected bone, which can often be better delineated with the use of intravenous contrast (Figures 18B-C) [14, 31, 33, 52, 75, 100]. Infected bone should have bone marrow oedema signal on fluid-sensitive images, and confluent low signal on T1W images (Figures 18B-D). Recent studies have shown that in patients with diabetic foot ulcers, bone marrow oedema with increased signal on fluid-sensitive sequences and preserved T1W signal frequently progresses to osteomyelitis, especially in ulcers larger than 3 cm that involve greater than 50% of subcutaneous fat or with a sinus tract extending to bone, and when the bone marrow fluid signal region of interest measurement to joint fluid region of interest measurement ratio is greater than 53% [52, 101-104]. Occasionally, there may be non-visualization of the cortical margins of the infected bone on the T1W images (known as the "ghost sign"), with the cortical margins visualized on both the fluid-sensitive and contrast-enhanced images, which may be helpful in the diagnosis of superimposed infection in a neuropathic foot [14, 31, 33, 41, 52, 100]. Septic arthritis is often present in infections of neuropathic feet, usually involving the metatarsophalangeal and interphalangeal joints [33, 34]. Other secondary signs that suggest the presence of osteomyelitis in a neuropathic foot include periosteal reaction, abscess formation, and tenosynovitis [34]. Intraarticular bone fragments and subchondral cyst-like changes are frequently associated with an uninfected neuropathic joint [31, 34, 41, 52, 100, 105]. MRI is extremely useful in delineating the extent of infection as well as osseous and soft-tissue viability, which can help minimize the extent of surgical resection [31, 34, 101]. Intravenous gadolinium-based contrast is not essential for the diagnosis of osteomyelitis, but it aids in the evaluation of abscess formation, sinus tracts, and necrotic bone [31, 101]. DWI and DCE MRI can also be helpful in evaluating superimposed infection in the neuropathic foot [14, 106, 107]. Osteomyelitis, due to the presence of inflammatory cells, pus, and detritus demonstrates greater restricted diffusion and lower ADC values on DWI than does diabetic neuropathy, where pure bone marrow oedema is present [32, 41, 107]. DCE MRI allows for evaluation of tissue perfusion, which can help to distinguish necrotic from viable tissues, and may help differentiate bone marrow oedema due to osteoarthritis from bone marrow oedema due to osteomyelitis [41].

Treatment of the infected diabetic foot ranges from intravenous antibiotics and wound care to surgical debridement and possible amputation [33, 108].

Conclusions

In 2021, the Society of Skeletal Radiology (SSR) Practice Guidelines and Technical Standards Committee (PGTSC)

Table 1. Methods of improving imaging when hardware present

Use vendor-specific metal artifact reduction
Use short tau inversion recovery (STIR) or DIXON for fat suppression
Use FAST SPIN ECHO (FSE) sequences; reduce echo spacing on FSE
Increase echo train length (ETL)
Reduce effective TE
Reduce slice thickness
Increase image resolution
Increase receiver bandwidth (BW); use high/fast gradient performance
Increase number of excitations (NEX); turn off parallel imaging
Align cylindrical implants parallel to the main magnetic field
Swap phase and frequency directions

assessed the literature and proposed standardized terminology for reporting imaging findings of infection on MRI [109]. Our paper largely follows their suggested guidelines, with a few minor differences. This consensus paper suggests reporting confluent subcutaneous edema as having either a high or low likelihood of cellulitis based on additional imaging findings, and reserving the term "cellulitis" for enhancing superficial soft tissues. The SSR PGTSC also discourages the use of the term "phlegmon", as it likely would not change clinical management, and advocate the use of "cellulitis, myositis, or fasciitis, without soft tissue abscess". This consensus paper also advises describing non-enhancing tissues underneath or beyond an ulcer margin as "devitalized tissue" to guide surgical resection. The authors of the consensus paper suggest using "necrotizing deep soft tissue infection" rather than "necrotizing fasciitis". They suggest using "periosteal reaction" to encompass the terms "periosteal reaction", "periostitis", and "periosteal new bone". They support the term "subperiosteal spread of infection" rather than "subperiosteal abscess". The authors of the consensus paper suggest avoiding the terms "osteitis" and "reactive marrow edema" for infection cases, and using these terms on for non-infection cases such as trauma and inflammatory arthritis.

MRI is a powerful imaging modality in the evaluation of various MSK soft tissue, joint, and bone infections, allowing prompt diagnosis and assessment of the extent of disease, permitting timely treatment and optimizing long-term clinical outcomes. This highly sensitive imaging modality is also very useful in monitoring response to treatment.

Conflict of interest

The authors declare that they have no conflict of interest.

References

1. Turecki MB, Taljanovic MS, Stubbs AY, et al. Imaging of musculoskeletal soft tissue infections. Skeletal Radiol 2010; 39: 957-971.
2. Headley AJ. Necrotizing soft tissue infections: a primary care review. Am Fam Physician 2003; 68: 323-328.
3. Hill MK, Sanders CV. Skin and soft tissue infections in critical care. Crit Care Clin 1998; 14: 251-262.
4. Expert Panel on Musculoskeletal Imaging; Beaman FD, von Herrmann PF, Kransdorf MJ, et al. ACR Appropriateness Criteria(®) suspected osteomyelitis, septic arthritis, or soft tissue infection (excluding spine and diabetic foot). J Am Coll Radiol 2017; 14 (5S): S326-S337.
5. Walker EA, Beaman FD, Wessell DE, et al. ACR Appropriateness Criteria® suspected osteomyelitis of the foot in patients with diabetes mellitus. J Am Coll Radiol 2019, 16 (11S): S440-S450.
6. Taljanovic MS, Hunter TB, Fitzpatrick KA, et al. Musculoskeletal magnetic resonance imaging: importance of radiography. Skeletal Radiol 2003; 32: 403-411.
7. Prodi E, Grassi R, Iacobellis F, Cianfoni A. Imaging in spondylodiskitis. Magn Reson Imaging Clin N Am 2016; 24: 581-600.
8. Kowalski TJ, Layton KF, Berbari EF, et al. Follow-up MR imaging in patients with pyogenic spine infections: lack of correlation with clinical features. AJNR Am J Neuroradiol 2007; 28: 693-699.
9. Love C, Palestro CJ. Nuclear medicine imaging of bone infections. Clin Radiol 2016; 71: 632-646.
10. Engin G, Acunaş B, Acunaş G, Tunaci M. Imaging of extrapulmonary tuberculosis. Radiographics 2000; 20: 471-488; quiz 529-430, 532.
11. Moon MS. Tuberculosis of the spine. Controversies and a new challenge. Spine (Phila Pa 1976) 1997; 22: 1791-1797.
12. Sanghvi DA, Iyer VR, Deshmukh T, Hoskote SS. MRI features of tuberculosis of the knee. Skeletal Radiol 2009; 38: 267-273.
13. Bariteau JT, Waryasz GR, McDonnell M, et al. Fungal osteomyelitis and septic arthritis. J Am Acad Orthop Surg 2014; 22: 390-401.
14. Mandell JC, Khurana B, Smith JT, et al. Osteomyelitis of the lower extremity: pathophysiology, imaging, and classification, with an emphasis on diabetic foot infection. Emerg Radiol 2018; 25: 175-188.
15. Chan BY, Crawford AM, Kobes PH, et al. Septic arthritis: an evidence-based review of diagnosis and image-guided aspiration. AJR Am J Roentgenol 2020; 215: 568-581.
16. Offiah AC. Acute osteomyelitis, septic arthritis and discitis: differences between neonates and older children. Eur J Radiol 2006; 60: 221-232.
17. Gilbertson-Dahdal D, Wright JE, Krupinski E, et al. Transphyseal involvement of pyogenic osteomyelitis is considerably more common than classically taught. AJR Am J Roentgenol 2014; 203: 190-195.
18. Perlman MH, Patzakis MJ, Kumar PJ, Holtom P. The incidence of joint involvement with adjacent osteomyelitis in pediatric patients. J Pediatr Orthop 2000; 20: 40-43.
19. Schallert EK, Kan JH, Monsalve J, et al. Metaphyseal osteomyelitis in children: how often does MRI-documented joint effusion or epiphyseal extension of edema indicate coexisting septic arthritis? Pediatr Radiol 2015; 45: 1174-1181.
20. Peltola H, Pääkkönen M. Acute osteomyelitis in children. N Engl J Med 2014; 370: 352-360.
21. Raff AB, Kroshinsky D. Cellulitis: a review. JAMA 2016; 316: 325-337.
22. Ali SZ, Srinivasan S, Peh WC. MRI in necrotizing fasciitis of the extremities. Br J Radiol 2014; 87: 20130560.
23. Mehta P, Morrow M, Russell J, et al. Magnetic resonance imaging of musculoskeletal emergencies. Semin Ultrasound CT MR 2017; 38: 439-452.
24. Yu JS, Habib P. MR imaging of urgent inflammatory and infectious conditions affecting the soft tissues of the musculoskeletal system. Emerg Radiol 2009; 16: 267-276.
25. Altmayer S, Verma N, Dicks EA, Oliveira A. Imaging musculoskeletal soft tissue infections. Semin Ultrasound CT MR 2020; 41: 85-98.
26. Hayeri MR, Ziai P, Shehata ML, et al. Soft-tissue infections and their imaging mimics: from cellulitis to necrotizing fasciitis. Radiographics 2016; 36: 1888-1910.
27. Swartz MN. Clinical practice. Cellulitis. N Engl J Med 2004; 350: 904-912.
28. Kirchgesner T, Tamigneaux C, Acid S, et al. Fasciae of the musculoskeletal system: MRI findings in trauma, infection and neoplastic diseases. Insights Imaging 2019; 10: 47.

29. Chaudhry AA, Baker KS, Gould ES, Gupta R. Necrotizing fasciitis and its mimics: what radiologists need to know. AJR Am J Roentgenol 2015; 204: 128-139.
30. Christian S, Kraas J, Conway WF. Musculoskeletal infections. Semin Roentgenol 2007; 42: 92-101.
31. Donovan A, Schweitzer ME. Use of MR imaging in diagnosing diabetes-related pedal osteomyelitis. Radiographics 2010; 30: 723-736.
32. Kumar Y, Khaleel M, Boothe E, et al. Role of diffusion weighted imaging in musculoskeletal infections: current perspectives. Eur Radiol 2017; 27: 414-423.
33. Leone A, Vitiello C, Gullì C, et al. Bone and soft tissue infections in patients with diabetic foot. Radiol Med 2020; 125: 177-187.
34. Leone A, Cassar-Pullicino VN, Semprini A, et al. Neuropathic osteoarthropathy with and without superimposed osteomyelitis in patients with a diabetic foot. Skeletal Radiol 2016; 45: 735-754.
35. Beltran J. MR imaging of soft-tissue infection. Magn Reson Imaging Clin N Am 1995; 3: 743-751.
36. Ma LD, Frassica FJ, Bluemke DA, Fishman EK. CT and MRI evaluation of musculoskeletal infection. Crit Rev Diagn Imaging 1997; 38: 535-568.
37. Struk DW, Munk PL, Lee MJ, et al. Imaging of soft tissue infections. Radiol Clin North Am 2001; 39: 277-303.
38. McGuinness B, Wilson N, Doyle AJ. The "penumbra sign" on T1-weighted MRI for differentiating musculoskeletal infection from tumour. Skeletal Radiol 2007; 36: 417-421.
39. Moritani T, Kim J, Capizzano AA, et al. Pyogenic and non-pyogenic spinal infections: emphasis on diffusion-weighted imaging for the detection of abscesses and pus collections. Br J Radiol 2014; 87: 20140011.
40. Winegar BA, Kay MD, Taljanovic M. Magnetic resonance imaging of the spine. Pol J Radiol 2020; 85: e550-e574.
41. Martín Noguerol T, Luna Alcalá A, Beltrán LS, et al. Advanced MR Imaging Techniques for Differentiation of Neuropathic Arthropathy and Osteomyelitis in the Diabetic Foot. Radiographics 2017; 37: 1161-1180.
42. Harish S, Chiavaras MM, Kotnis N, Rebello R. MR imaging of skeletal soft tissue infection: utility of diffusion-weighted imaging in detecting abscess formation. Skeletal Radiol 2011; 40: 285-294.
43. Gordon BA, Martinez S, Collins AJ. Pyomyositis: characteristics at CT and MR imaging. Radiology 1995; 197: 279-286.
44. Trusen A, Beissert M, Schultz G, et al. Ultrasound and MRI features of pyomyositis in children. Eur Radiol 2003; 13: 1050-1055.
45. Crum NF. Bacterial pyomyositis in the United States. Am J Med 2004; 117: 420-428.
46. Fountoukis T, Tsatsanidis N, Tilkeridou M, et al. Abdominal rectus muscle pyomyositis: Report of a case and review of the literature. Infect Dis Rep 2018; 10: 7522.
47. Comegna L, Guidone PI, Prezioso G, et al. Pyomyositis is not only a tropical pathology: a case series. J Med Case Rep 2016; 10: 372.
48. Khoshhal K, Abdelmotaal HM, Alarabi R. Primary obturator internus and obturator externus pyomyositis. Am J Case Rep 2013; 14: 94-98.
49. Kattapuram TM, Suri R, Rosol MS, et al. Idiopathic and diabetic skeletal muscle necrosis: evaluation by magnetic resonance imaging. Skeletal Radiol 2005; 34: 203-209.
50. Kapur S, Brunet JA, McKendry RJ. Diabetic muscle infarction: case report and review. J Rheumatol 2004; 31: 190-194.
51. Cunningham J, Sharma R, Kirzner A, et al. Acute myonecrosis on MRI: etiologies in an oncological cohort and assessment of interobserver variability. Skeletal Radiol 2016; 45: 1069-1078.
52. Baker JC, Demertzis JL, Rhodes NG, et al. Diabetic musculoskeletal complications and their imaging mimics. Radiographics 2012; 32: 1959-1974.
53. Schmid MR, Kossmann T, Duewell S. Differentiation of necrotizing fasciitis and cellulitis using MR imaging. AJR Am J Roentgenol 1998; 170: 615-620.
54. Fugitt JB, Puckett ML, Quigley MM, Kerr SM. Necrotizing fasciitis. Radiographics 2004; 24: 1472-1476.
55. Brothers TE, Tagge DU, Stutley JE, et al. Magnetic resonance imaging differentiates between necrotizing and non-necrotizing fasciitis of the lower extremity. J Am Coll Surg 1998; 187: 416-421.
56. Tso DK, Singh AK. Necrotizing fasciitis of the lower extremity: imaging pearls and pitfalls. Br J Radiol 2018; 91: 20180093.
57. Malghem J, Lecouvet FE, Omoumi P, et al. Necrotizing fasciitis: contribution and limitations of diagnostic imaging. Joint Bone Spine 2013; 80: 146-154.
58. Kim MC, Kim S, Cho EB, et al. Utility of magnetic resonance imaging for differentiating necrotizing fasciitis from severe cellulitis: a magnetic resonance indicator for necrotizing fasciitis (MRINEC) algorithm. J Clin Med 2020; 9: 3040.
59. Sarani B, Strong M, Pascual J, Schwab CW. Necrotizing fasciitis: current concepts and review of the literature. J Am Coll Surg 2009; 208: 279-288.
60. Beauchamp NJ Jr, Scott WW Jr, Gottlieb LM, Fishman EK. CT evaluation of soft tissue and muscle infection and inflammation: a systematic compartmental approach. Skeletal Radiol 1995; 24: 317-324.
61. Kothari NA, Pelchovitz DJ, Meyer JS. Imaging of musculoskeletal infections. Radiol Clin North Am 2001; 39: 653-671.
62. Kim KT, Kim YJ, Won Lee J, et al. Can necrotizing infectious fasciitis be differentiated from nonnecrotizing infectious fasciitis with MR imaging? Radiology 2011; 259: 816-824.
63. Baumbach SF, Lobo CM, Badyine I, et al. Prepatellar and olecranon bursitis: literature review and development of a treatment algorithm. Arch Orthop Trauma Surg 2014; 134: 359-370.
64. Khodaee M. Common superficial bursitis. Am Fam Physician 2017; 95: 224-231.
65. Zimmermann B 3rd, Mikolich DJ, Ho G Jr. Septic bursitis. Semin Arthritis Rheum 1995; 24: 391-410.
66. Lormeau C, Cormier G, Sigaux J, et al. Management of septic bursitis. J Bone Spine 2019; 86: 583-588.
67. Deal JB Jr, Vaslow AS, Bickley RJ, et al. Empirical treatment of uncomplicated septic olecranon bursitis without aspiration. J Hand Surg Am 2020; 45: 20-25.
68. Small LN, Ross JJ. Suppurative tenosynovitis and septic bursitis. Infect Dis Clin North Am 2005; 19: 991-1005, xi.
69. Bureau NJ, Chhem RK, Cardinal E. Musculoskeletal infections: US manifestations. Radiographics 1999; 19: 1585-1592.
70. Chapman T, Ilyas AM. Pyogenic flexor tenosynovitis: evaluation and treatment strategies. J Hand Microsurg 2019; 11: 121-126.
71. Hausman MR, Lisser SP. Hand infections. Orthop Clin North Am 1992; 23: 171-185.
72. Kano Y, Momose T. Acute lymphangitis. Cleve Clin J Med 2020; 87: 129-130.
73. Falagas ME, Bliziotis IA, Kapaskelis AM. Red streaks on the leg. Lymphangitis. Am Fam Physician 2006; 73: 1061-1062.
74. Morgan R, Teh J, Craze J, Sadarangani M. Unusual cause of lymphangitis in a 2-year-old boy. BMJ Case Rep 2016; 2016: bcr2016215058.

75. Anwer U, Yablon CM. Imaging of osteomyelitis of the extremities. Semin Roentgenol 2017; 52: 49-54.
76. Jennin F, Bousson V, Parlier C, et al. Bony sequestrum: a radiologic review. Skeletal Radiol 2011; 40: 963-975.
77. Weenders SG, Janssen NE, Landman GW, van den Berg FP. Subperiosteal abscess in a child. Trueta's osteomyelitis hypothesis undermined? Orthop Traumatol Surg Res 2015; 101: 763-765.
78. Yeo A, Ramachandran M. Acute haematogenous osteomyelitis in children. BMJ 2014; 348: g66.
79. Llewellyn A, Jones-Diette J, Kraft J, et al. Imaging tests for the detection of osteomyelitis: a systematic review. Health Technol Assess 2019; 23: 1-128.
80. Llewellyn A, Kraft J, Holton C, et al. Imaging for detection of osteomyelitis in people with diabetic foot ulcers: a systematic review and meta-analysis. Eur J Radiol 2020; 131: 109215.
81. Grey AC, Davies AM, Mangham DC, et al. The 'penumbra sign' on T1-weighted MR imaging in subacute osteomyelitis: frequency, cause and significance. Clin Radiol 1998; 53: 587-592.
82. Patel KB, Poplawski MM, Pawha PS, et al. Diffusion-weighted MRI "claw sign" improves differentiation of infectious from degenerative modic type 1 signal changes of the spine. AJNR Am J Neuroradiol 2014; 35: 1647-1652.
83. Roderick MR, Shah R, Rogers V, et al. Chronic recurrent multifocal osteomyelitis (CRMO) – advancing the diagnosis. Pediatr Rheumatol Online J 2016; 14: 47.
84. Roerdink RL, Huijbregts H, van Lieshout AWT, et al. The difference between native septic arthritis and prosthetic joint infections: A review of literature. J Orthop Surg (Hong Kong) 2019; 27: 2309499019860468.
85. Graif M, Schweitzer ME, Deely D, Matteucci T. The septic versus nonseptic inflamed joint: MRI characteristics. Skeletal Radiol 1999; 28: 616-620.
86. Chen WL, Chang WN, Chen YS, et al. Acute community-acquired osteoarticular infections in children: high incidence of concomitant bone and joint involvement. J Microbiol Immunol Infect 2010; 43: 332-338.
87. Montgomery CO, Siegel E, Blasier RD, Suva LJ. Concurrent septic arthritis and osteomyelitis in children. J Pediatr Orthop 2013; 33: 464-467.
88. Nguyen A, Kan JH, Bisset G, Rosenfeld S. Kocher criteria revisited in the era of MRI: how often does the kocher criteria identify underlying osteomyelitis? J Pediatr Orthop 2017; 37: e114-e119.
89. Kocher MS, Zurakowski D, Kasser JR. Differentiating between septic arthritis and transient synovitis of the hip in children: an evidence-based clinical prediction algorithm. J Bone Joint Surg Am 1999; 81: 1662-1670.
90. Karchevsky M, Schweitzer ME, Morrison WB, Parellada JA. MRI findings of septic arthritis and associated osteomyelitis in adults. AJR Am J Roentgenol 2004; 182: 119-122.
91. Porrino J, Wang A, Moats A, et al. Prosthetic joint infections: diagnosis, management, and complications of the two-stage replacement arthroplasty. Skeletal Radiol 2020; 49: 847-859.
92. Cyteval C, Bourdon A. Imaging orthopedic implant infections. Diagn Interv Imaging 2012; 93: 547-557.
93. Mar WA, Tan I, Song A, et al. Update on imaging of knee arthroplasties: normal findings and hardware complications. Semin Musculoskelet Radiol 2019; 23: e20-e35.
94. Plodkowski AJ, Hayter CL, Miller TT, et al. Lamellated hyperintense synovitis: potential MR imaging sign of an infected knee arthroplasty. Radiology 2013; 266: 256-260.
95. Li AE, Sneag DB, Greditzer HG 4th, et al. Total knee arthroplasty: diagnostic accuracy of patterns of synovitis at MR imaging. Radiology 2016; 281: 499-506.
96. Winegar BA, Kay MD, Chadaz TS, et al. Update on imaging of spinal fixation hardware. Semin Musculoskelet Radiol 2019; 23: e56-e79.
97. Bonnevialle P. Operative treatment of early infection after internal fixation of limb fractures (exclusive of severe open fractures). Orthop Traumatol Surg Res 2017; 103 (1S): S67-S73.
98. Otto-Lambertz C, Glauner A, Yagdiran A, Eysel P. Periprosthetic infections: How do we diagnose and treat? Results of an online survey and comparison with international recommendations. Orthop Surg 2021; 13: 1639-1645.
99. Trampuz A, Zimmerli W. Diagnosis and treatment of infections associated with fracture-fixation devices. Injury 2006; 37 Suppl 2: S59-S66.
100. Toledano TR, Fatone EA, Weis A, et al. MRI evaluation of bone marrow changes in the diabetic foot: a practical approach. Semin Musculoskelet Radiol 2011; 15: 257-268.
101. Gorbachova T. Magnetic resonance imaging of the ankle and foot. Pol J Radiol 2020; 85: e532-e549.
102. Sax AJ, Halpern EJ, Zoga AC, et al. Predicting osteomyelitis in patients whose initial MRI demonstrated bone marrow edema without corresponding T1 signal marrow replacement. Skeletal Radiol 2020; 49: 1239-1247.
103. Duryea D, Bernard S, Flemming D, et al. Outcomes in diabetic foot ulcer patients with isolated T2 marrow signal abnormality in the underlying bone: should the diagnosis of "osteitis" be changed to "early osteomyelitis"? Skeletal Radiol 2017; 46: 1327-1333.
104. Jang YH, Park S, Park YU, et al. Multivariate analyses of MRI findings for predicting osteomyelitis of the foot in diabetic patients. Acta Radiol 2020; 61: 1205-1212.
105. Ahmadi ME, Morrison WB, Carrino JA, et al. Neuropathic arthropathy of the foot with and without superimposed osteomyelitis: MR imaging characteristics. Radiology 2006; 238: 622-631.
106. Diez AIG, Fuster D, Morata L, et al. Comparison of the diagnostic accuracy of diffusion-weighted and dynamic contrast-enhanced MRI with (18)F-FDG PET/CT to differentiate osteomyelitis from Charcot neuro-osteoarthropathy in diabetic foot. Eur J Radiol 2020; 132: 109299.
107. Abdel Razek AAK, Samir S. Diagnostic performance of diffusion-weighted MR imaging in differentiation of diabetic osteoarthropathy and osteomyelitis in diabetic foot. Eur J Radiol 2017; 89: 221-225.
108. Noor S, Khan RU, Ahmad J. Understanding diabetic foot infection and its management. Diabetes Metab Syndr 2017; 11: 149-156.
109. Alaia EF, Chhabra A, Simpfendorfer CS, et al. MRI nomenclature for musculoskeletal infection. Skeletal Radiol 2021; 50: 2319-2347.